The mTORC1-mediated activation of ATF4 promotes protein and glutathione synthesis downstream of growth signals

Margaret E. Torrence[1], Michael R. MacArthur[1], Aaron M. Hosios[1], Alexander J. Valvezan[2], John M. Asara[3], James R. Mitchell[1,4], Brendan D. Manning[1, †]

[1] Department of Molecular Metabolism, Harvard T. H. Chan School of Public Health, Boston, MA 02115, USA

[2] Center for Advanced Biotechnology and Medicine, Department of Pharmacology, Rutgers Robert Wood Johnson Medical School, Piscataway, NJ 08854, USA

[3] Division of Signal Transduction, Beth Israel Deaconess Medical Center and Department of Medicine, Harvard Medical School, Boston, MA 02115, USA

[4] Department of Health Sciences and Technology, Swiss Federal Institute of Technology (ETH) Zurich, Schwerzenbach, Switzerland

[†] Corresponding author. E-mail: bmanning@hsph.harvard.edu

Abstract

The mechanistic target of rapamycin complex 1 (mTORC1) stimulates a coordinated anabolic program in response to growth-promoting signals. Paradoxically, recent studies indicate that mTORC1 can activate the adaptive stress-responsive transcription factor ATF4 through mechanisms distinct from its canonical induction by the integrated stress response (ISR). However, how ATF4 functions in response to these distinct modes of regulation and its broader role as a downstream target of mTORC1 are unknown. Therefore, we directly compared ATF4-dependent transcriptional changes induced upon activation of mTORC1 or the ISR. The mTORC1-ATF4 pathway stimulated the expression of only a subset of the ATF4 target genes stimulated by the ISR, including genes involved in amino acid uptake, synthesis, and tRNA charging. We demonstrate that ATF4 is a metabolic effector of mTORC1 involved in both its established role in promoting protein synthesis and in a previously unappreciated function for mTORC1 in stimulating cellular cystine uptake and glutathione synthesis.

Introduction

Pro-growth signals in the form of growth factors, hormones, and nutrients impinge on cellular metabolic programs in a coordinated fashion involving both acute, post-translational regulation and transcriptional control of nutrient transporters and metabolic enzymes. The mechanistic target of rapamycin complex 1 (mTORC1) acts as a central point of integration for these signals and propagates a downstream metabolic response that increases anabolic processes while decreasing specific catabolic processes. Through a variety of downstream effectors, mTORC1 stimulates the synthesis of the major macromolecules comprising cellular biomass, including protein, lipid, and nucleotides, along with metabolic and adaptive pathways that support this anabolic program (Valvezan & Manning, 2019).

One particularly interesting feature of this coordinated metabolic program that has emerged in recent years is that the mTORC1 signaling pathway can co-opt key nutrient-sensing transcription factors that are activated, independent of mTORC1, in response to depletion of nutrients. In their canonical roles, these transcription factors serve to mount an adaptive response by upregulating genes that allow cells to overcome the specific nutrient deficiency. The best characterized of these transcription factors with dual regulation is the hypoxia-inducible factor 1 (HIF1) comprising the rapidly turning over HIF1α protein heterodimerized with the stable aryl hydrocarbon receptor nuclear translocator (ARNT or HIF1β). Hypoxia (a decrease in oxygen) rapidly stabilizes HIF1α and allows the HIF1 heterodimer to induce genes involved in glucose uptake, glycolysis, and angiogenesis to adapt to hypoxia and decrease capacity for mitochondrial respiration (Nakazawa et al., 2016). While this regulation is entirely independent of mTORC1 (Arsham et al., 2002), in response to upstream growth factors and oncogenes, activation of mTORC1 stimulates an increase in HIF1α via enhanced cap-dependent translation of the HIF1α mRNA, which is sufficient to stimulate an increase in glucose uptake and glycolysis even when oxygen is not limiting (e.g. normoxia), a process referred to as aerobic glycolysis, which supports the production of biosynthetic precursors in the form

56 of glycolytic intermediates (Brugarolas et al., 2003; Duvel et al., 2010; Hudson et al., 2002;
57 Laughner et al., 2001; Thomas et al., 2006; Zhong et al., 2000).

58 Similarly, the sterol regulatory element (SRE)-binding protein (SREBP) family of
59 transcription factors are independently regulated by both adaptive nutrient signals and
60 growth signals controlling mTORC1. The SREBPs are canonically activated upon sterol
61 depletion, which promotes their trafficking from the endoplasmic reticulum (ER)
62 membrane to the Golgi apparatus, where they are proteolytically processed to release
63 the active transcription factor that translocates to the nucleus to induce genes with SREs,
64 including those encoding the enzymes required for de novo synthesis of fatty acid and
65 sterol lipids (Horton et al., 2002). In addition to this adaptive response, growth signaling
66 induces lipid synthesis via mTORC1-stimulated processing and activation of SREBP and
67 its lipogenic program through mechanisms that remain incompletely defined (Duvel et al.,
68 2010; Owen et al., 2012; Peterson et al., 2011; Porstmann et al., 2008). Recent studies
69 have suggested that the regulation of nutrient sensing transcription factors by both
70 adaptive and pro-growth signals extends to the transcription factor activating transcription
71 factor 4 (ATF4) (Ben-Sahra et al., 2016; Torrence & Manning, 2018).

72 ATF4 is a basic leucine zipper (bZIP) transcription factor that is selectively translated in
73 response to specific forms of cellular stress to induce the expression of genes involved in
74 adaptation to stress (Walter & Ron, 2011). This adaptive program is referred to as the
75 integrated stress response (ISR) and is initiated by stress-activated protein kinases,
76 including general control nonderepressible 2 (GCN2) activated upon amino acid
77 deprivation and protein kinase RNA-like endoplasmic reticulum kinase (PERK) activated
78 by ER stress, which phosphorylate eIF2α on Ser51 (Harding et al., 2000).
79 Phosphorylation of eIF2α serves to globally attenuate mRNA translation to conserve
80 amino acids and energy and decrease the cellular protein load as one adaptive measure
81 to overcome these stresses (Clemens, 1996). Importantly, a small number of mRNAs,
82 including that encoding ATF4, exhibit increased translation upon eIF2α-Ser51
83 phosphorylation (Vattem & Wek, 2004). The stress-induced increase in ATF4 leads to the
84 expression of a canonical set of ATF4 target genes, including those involved in non-

85 essential amino acid biosynthesis and amino acid transport, as part of the adaptive
86 cellular response specific to stresses such as amino acid depletion (Harding et al., 2003).

87 While ATF4 is a major downstream effector of the ISR, evidence is emerging that ATF4
88 can also be activated by pro-growth signals that stimulate mTORC1 signaling (Adams,
89 2007; Ben-Sahra et al., 2016), and cis-regulatory elements for ATF4 binding are enriched
90 in the promoters of mTORC1-induced genes (Duvel et al., 2010). Importantly, the
91 mTORC1-mediated activation of ATF4 involves its increased translation in a manner that
92 is independent of the ISR and phosphorylation of eIF2α (Ben-Sahra et al., 2016; Park et
93 al., 2017). These findings suggest that, similar to HIF1 and SREBP, ATF4 induction may
94 be mobilized as part of the broader anabolic program downstream of mTORC1. Indeed,
95 our previous findings indicate that mTORC1 promotes *de novo* purine synthesis, in part,
96 through induction of mitochondrial one-carbon metabolism via ATF4 activation and
97 expression of its gene target MTHFD2 (Ben-Sahra et al., 2016).

98 How the ATF4-dependent gene program compares between its adaptive role in the ISR
99 and its activation as a downstream effector of mTORC1 signaling and whether ATF4
100 contributes to established or new functions of mTORC1 are unknown (Figure 1A). Here,
101 we find that the mTORC1-ATF4 program represents a small subset of ATF4-dependent
102 genes induced by ER stress and includes genes encoding the enzymes required for tRNA
103 charging, non-essential amino acid synthesis, and amino acid uptake. Consistent with
104 regulation of these enzymes by mTORC1 through ATF4, ATF4 contributes to the
105 induction of protein synthesis downstream of mTORC1. We also find that mTORC1
106 signaling promotes glutathione synthesis through ATF4 and its specific regulation of the
107 cystine transporter SLC7A11. Thus, ATF4 is an anabolic effector of mTORC1 signaling,
108 necessary for both its canonical regulation of protein synthesis and its synthesis of
109 glutathione, the most abundant anti-oxidant in cells.

Results

mTORC1 signaling activates a subset of ATF4-dependent genes also activated by the integrated stress response

To identify the ATF4-dependent gene targets downstream of mTORC1, we compared the insulin-induced, rapamycin-sensitive transcripts between wild-type MEFs and those with biallelic loss of ATF4 via CRISPR/Cas9 gene deletion (see methods). Consistent with our previous studies (Ben-Sahra et al., 2016), insulin stimulated an increase in ATF4 protein in MEFs, which was blocked by rapamycin (Figure 1B). In parallel, these cells were treated with a time course of tunicamycin, an inhibitor of N-glycosylation that potently induces ER stress and an increase in ATF4, to identify ATF4 gene targets downstream of the ISR. 20% of transcripts (253 total) significantly upregulated upon insulin stimulation were significantly blocked in their induction with rapamycin treatment. Importantly, approximately 30% of these mTORC1-regulated genes (77 total) lost their insulin responsiveness with ATF4 deletion. In comparison, 36% of transcripts significantly induced with tunicamycin treatment at 4 hours were dependent on ATF4 (774 total). The expression of just 61 genes was found to overlap between these two modes of ATF4 regulation, being ATF4 dependent in response to both mTORC1 activation and the ISR (Figure 1C).

The RNA-seq analysis demonstrated that only a small subset of ATF4 gene targets induced by ER stress were also stimulated by mTORC1 signaling. Interestingly, these 61 shared genes showed significant KEGG pathway enrichment of aminoacyl tRNA biosynthesis, amino acid metabolism, and one-carbon metabolism (Figure 1D). Gene sets corresponding to these pathways were significantly enriched among the insulin-induced, rapamycin-sensitive genes (Figure 1E—figure supplement 1A). Amongst the 61 shared ATF4-dependent transcripts, those involved in amino acid synthesis and transport, one-carbon metabolism, and aminoacyl tRNA charging showed largely comparable fold-changes between insulin stimulation and tunicamycin treatment, while canonical genes of the ER stress response, such as *Herpud1* and *Ddit3/Chop,* showed much greater induction with tunicamycin (Figure 1F). In addition to aminoacyl tRNA synthetase genes,

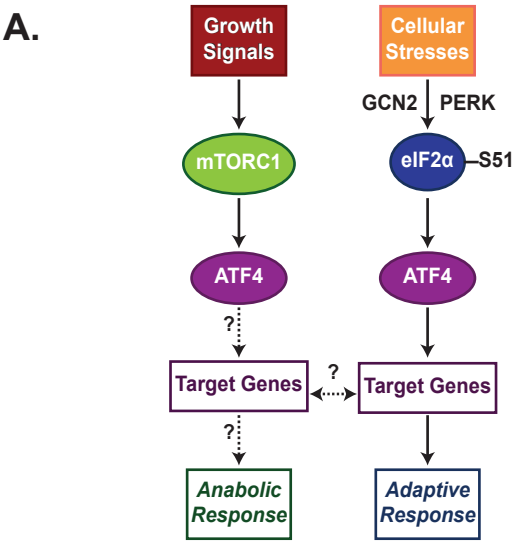

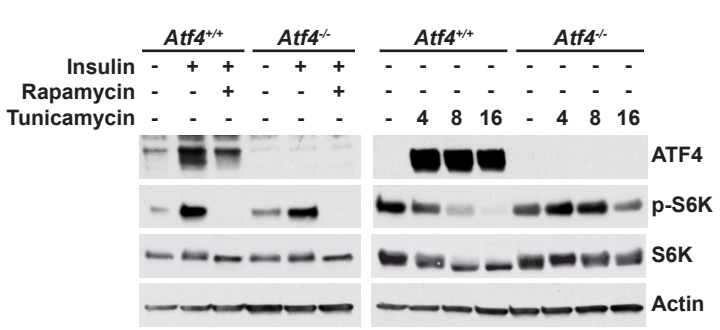

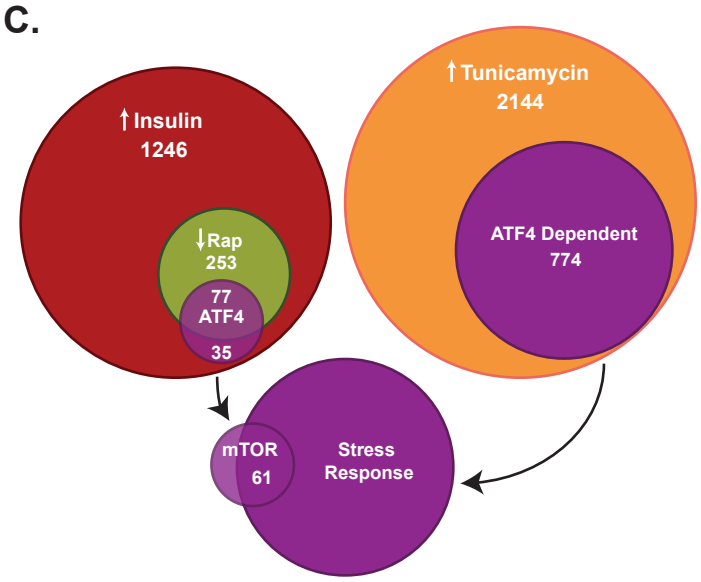

D.

Shared mTORC1 and ISR KEGG Enrichment

Function	P Value
Aminoacyl tRNA Biosynthesis	1.19E-07
Gly, Ser, and Thr Metabolism	7.85E-05
1-Carbon Metabolism	7.85E-05
Cys and Met Metabolism	.0001894
Ala, Asp, and Gln Metabolism	.01337497

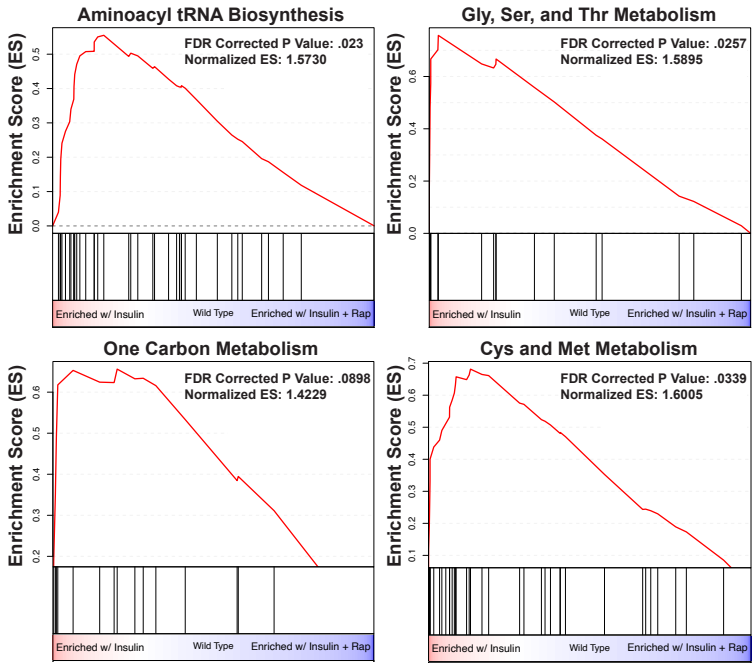

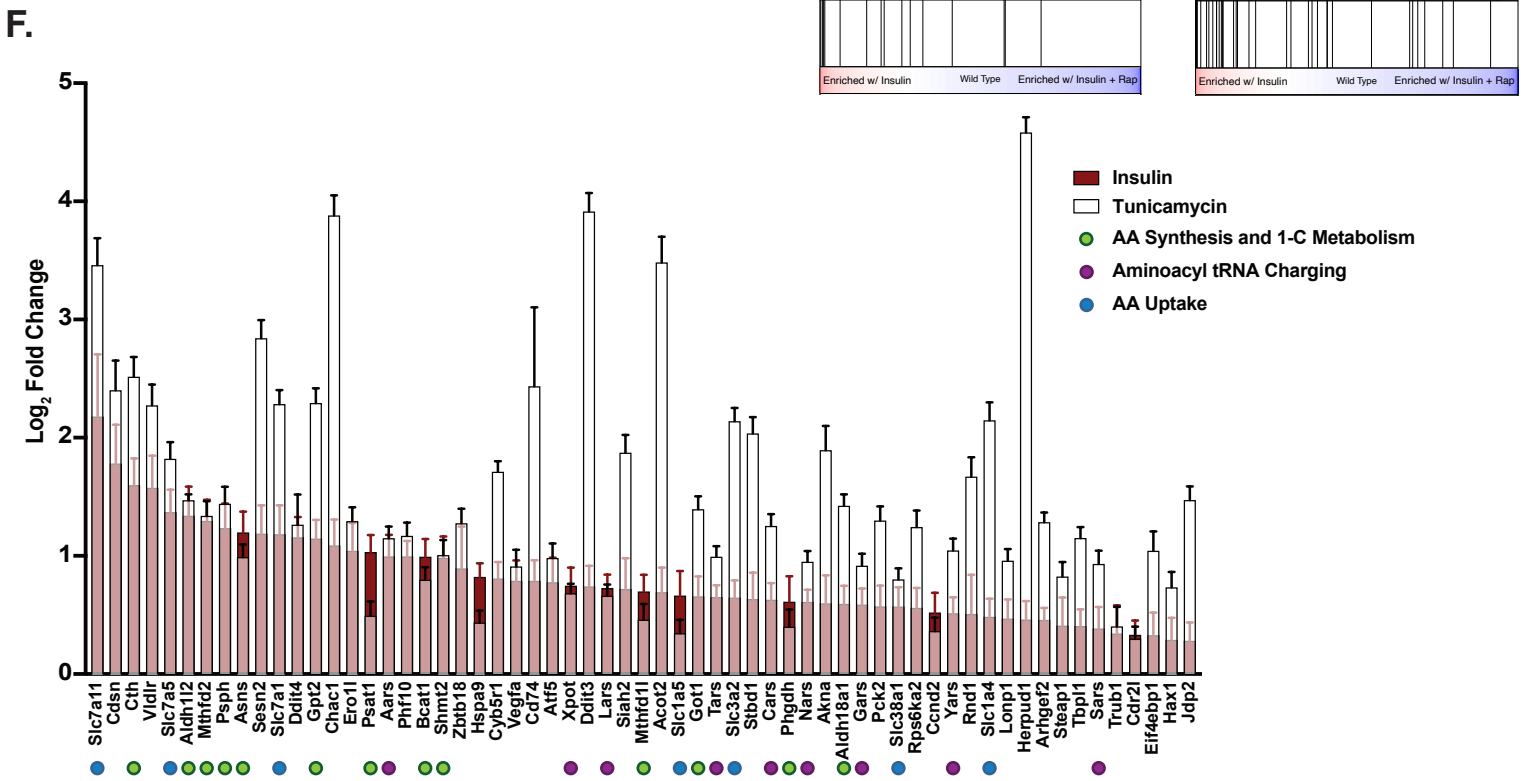

Figure 1. mTORC1 signaling activates a subset of ATF4-dependent genes also activated by the integrated stress response.

(A) Schematic of the dual regulation of ATF4 and the unknowns addressed in this study.

(B) Immunoblots of parallel lysates from RNA-Seq experiment. *Atf4*$^{+/+}$ and *Atf4*$^{-/-}$ MEFs were treated, as indicated, with insulin (500 nM, 16 h) or rapamycin (20 nM, 30 min) prior to insulin (Left) or with tunicamycin (2 μg/mL) for 4, 8 or 16 h (Right).

(C) Venn diagram depicting number and overlap of mTORC1- and ISR-induced transcripts, including those increased with insulin (red), decreased relative to insulin with rapamycin (green), and increased with 4 h tunicamycin (orange), and those dependent on ATF4 within these categories (purple), all with *P* values < 0.05. Only 61 ATF4-dependent genes overlap between those induced by insulin in a rapamycin-sensitive manner and those induced by tunicamycin. Gene lists per category are provided in Source data 1.

(D) KEGG enrichment of the shared mTORC1- and ISR-induced ATF4 target genes. *P* values were false discovery rate corrected (FDR).

(E) GSEA plots of mTORC1-induced genes dependent on ATF4 are shown. *P* values were FDR corrected and enrichment scores (ES) were normalized to total read count. Additional GSEA plot of alanine, aspartate, and glutamate metabolism is provided in figure supplement 1.

(F) The 61 ATF4-dependent genes induced by both mTORC1 (i.e., rapamycin-sensitive insulin stimulation) and tunicamycin treatment are shown ranked from left to right in order of greatest $\log_2$-fold change with insulin (red bars), with the corresponding tunicamycin-induced changes superimposed (white bars) (n = 4). Error bars depict 95% confidence intervals.

expression of the *Xpot* gene encoding Exportin-T, which is the major Ran GTPase family member for nuclear to cytosolic export of mature tRNAs (Arts et al., 1998; Kutay et al., 1998), was found to be similarly regulated by ATF4 in response to mTORC1 and ISR activation. Genes encoding known negative regulators of mTORC1 signaling are also among these 61 shared genes, including *Ddit4/Redd1* and *Sesn2*. These targets likely contribute to the ATF4-dependent inhibition of mTORC1 signaling (S6K1 phosphorylation) detected upon tunicamycin treatment (Figure 1B), while in the context of mTORC1 signaling, these ATF4 targets might play a role in negative feedback regulation of mTORC1. These data suggest that a specific subset of ATF4-dependent ISR-induced genes are likewise regulated by growth factor signaling through mTORC1 and are enriched for specific processes including aminoacyl tRNA biosynthesis, amino acid synthesis and uptake, and one-carbon metabolism.

175 **mTORC1 signaling induces a large number of genes involved in amino acid**
176 **synthesis, transport, and charging through ATF4 activation**

177 To validate and expand the findings from the RNA-seq analysis, a Nanostring codeset
178 was designed to simultaneously quantify transcripts of genes involved in the enriched
179 processes above (see methods). As positive and negative controls, respectively, we
180 included the glycolytic targets of HIF1, established previously to be regulated downstream
181 of mTORC1 (Duvel et al., 2010), and the mitochondrial tRNA synthetases, not believed
182 to be regulated by ATF4. Using this codeset, we analyzed gene expression in three
183 settings of mTORC1 activation: 1) wild-type MEFs stimulated with insulin in the presence
184 or absence of rapamycin, 2) growth factor-independent activation of mTORC1 via genetic
185 loss of the TSC protein complex in *Tsc2*$^{-/-}$ MEFs, and 3) *Tsc2*$^{-/-}$ MEFs with siRNA-
186 mediated knockdown of ATF4 (Figure 2A—figure supplement 2A and Source data 2).
187 ATF4 protein levels were robustly upregulated with either genetic or insulin-stimulated
188 mTORC1 activation in these settings, with both rapamycin and ATF4 targeting siRNAs
189 blocking this induction (Figure supplement 2A). Interestingly, the majority of transcripts
190 analyzed in the functional categories that encode enzymes of non-essential amino acid
191 synthesis, one-carbon metabolism, amino acid transporters, and cytosolic amino-acyl
192 tRNA synthetases (and *Xpot*) were increased with mTORC1 activation in a manner
193 sensitive to both rapamycin and siRNA-mediated knockdown of ATF4. However, the HIF1
194 targets of glycolysis were mTORC1-regulated but independent of ATF4, and transcripts
195 encoding the mitochondrial tRNA synthetases were neither mTORC1- nor ATF4-
196 regulated. We further confirmed the mTORC1- and ATF4-mediated regulation of a
197 representative subset of these transcripts via qPCR (Figure 2B-C—figure supplement
198 2C). Consistent with previous studies (Ben-Sahra et al., 2016; Park et al., 2017), both
199 ATF4 transcript and protein levels were induced by mTORC1 signaling in these settings
200 (Figure 2B-E). Transcriptional changes in ATF4 gene targets were reflected in
201 corresponding changes in the abundance of representative protein products, with varying
202 degrees of rapamycin sensitivity that likely reflect inherent differences in the turnover
203 rates of these proteins (Figure 2D-E). We next wanted to confirm that these mTORC1-
204 and ATF4-induced changes were independent of the ISR. While we have shown

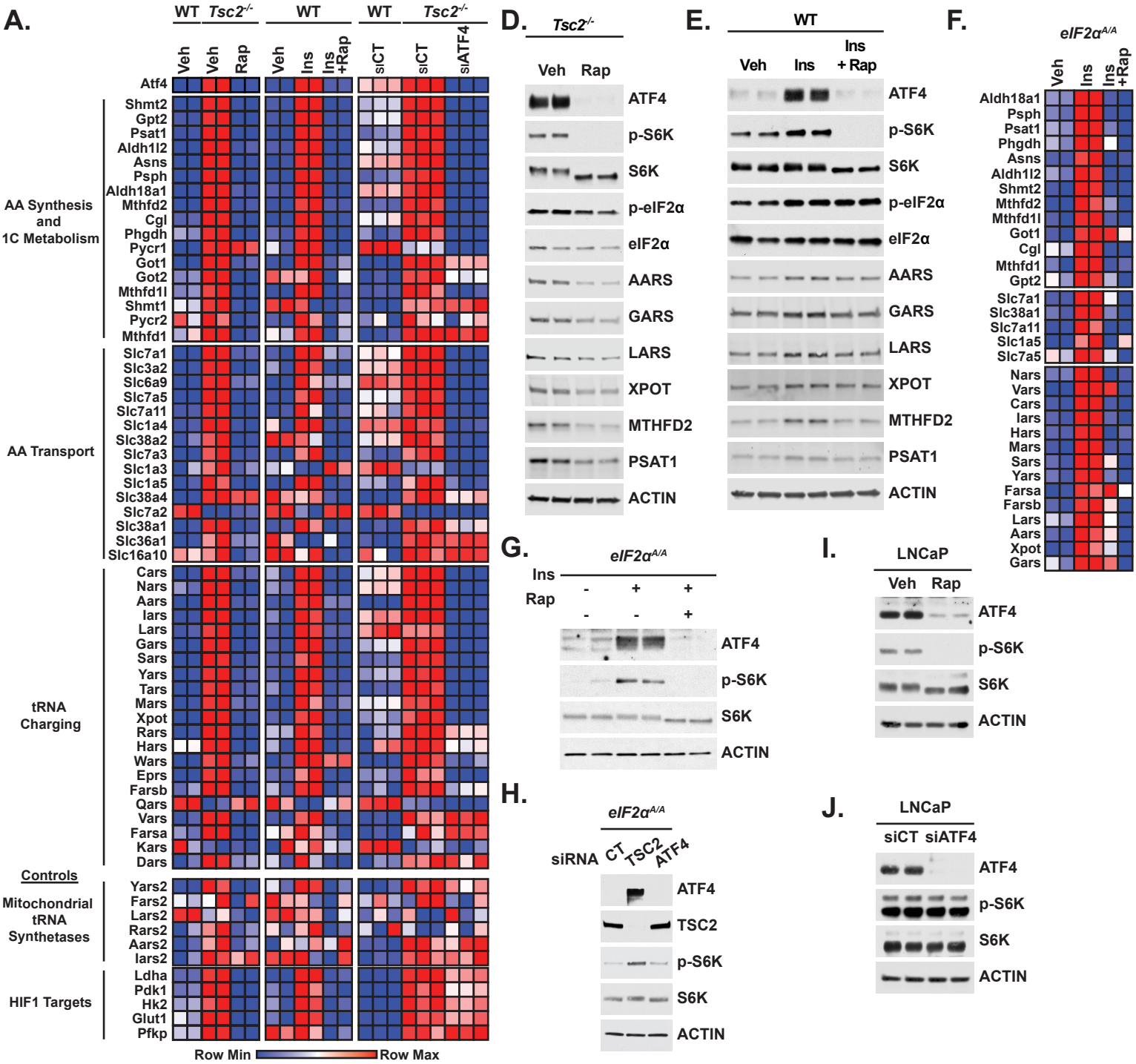
A.
WT
Tsc2-/-
WT
WT
Tsc2-/-
Veh
Veh
Rap
Veh
Ins
Ins +Rap
siCT
siCT
siATF4
Atf4
AA Synthesis and 1C Metabolism
Shmt2
Gpt2
Psat1
Aldh1l2
Asns
Psph
Aldh18a1
Mthfd2
Cgl
Phgdh
Pycr1
Got1
Got2
Mthfd1l
Shmt1
Pycr2
Mthfd1
AA Transport
Slc7a1
Slc3a2
Slc6a9
Slc7a5
Slc7a11
Slc1a4
Slc38a2
Slc7a3
Slc1a3
Slc1a5
Slc38a4
Slc7a2
Slc38a1
Slc36a1
Slc16a10
tRNA Charging
Cars
Nars
Aars
Iars
Lars
Gars
Sars
Yars
Tars
Mars
Xpot
Rars
Hars
Wars
Eprs
Farsb
Qars
Vars
Farsa
Kars
Dars
Controls
Mitochondrial tRNA Synthetases
Yars2
Fars2
Lars2
Rars2
Aars2
Iars2
HIF1 Targets
Ldha
Pdk1
Hk2
Glut1
Pfkp
Row Min
Row Max
D.
Tsc2-/-
Veh
Rap
ATF4
p-S6K
S6K
p-eIF2α
eIF2α
AARS
GARS
LARS
XPOT
MTHFD2
PSAT1
ACTIN
E.
WT
Veh
Ins
Ins + Rap
ATF4
p-S6K
S6K
p-eIF2α
eIF2α
AARS
GARS
LARS
XPOT
MTHFD2
PSAT1
ACTIN
F.
eIF2α A/A
Veh
Ins
Ins +Rap
Aldh18a1
Psph
Psat1
Phgdh
Asns
Aldh1l2
Shmt2
Mthfd2
Mthfd1l
Got1
Cgl
Mthfd1
Gpt2
Slc7a1
Slc38a1
Slc7a11
Slc1a5
Slc7a5
Nars
Vars
Cars
Iars
Hars
Mars
Sars
Yars
Farsa
Farsb
Lars
Aars
Xpot
Gars
G.
eIF2α A/A
Ins
Rap
ATF4
p-S6K
S6K
ACTIN
I.
LNCaP
Veh
Rap
ATF4
p-S6K
S6K
ACTIN
H.
eIF2α A/A
siRNA
CT
TSC2
ATF4
ATF4
TSC2
p-S6K
S6K
ACTIN
J.
LNCaP
siCT
siATF4
ATF4
p-S6K
S6K
ACTIN
B.
Relative Expression
Veh
Veh
Rap
WT
Tsc2-/-
Atf4
Psat1
Mthfd2
Slc7a5
Aars
Gars
C.
Relative Expression
Veh
Ins
Ins + Rap
Atf4
Psat1
Mthfd2
Slc7a5
Aars
Gars
K.
Relative Expression
LNCaP
Veh
Rap
PSAT1
ASNS
MTHFD2
SLC7A5
AARS
GARS
XPOT
L.
Relative Expression
LNCaP
siCT
siATF4
PSAT1
ASNS
MTHFD2
SLC7A5
AARS
GARS
XPOT

Figure 2. mTORC1 and ATF4 regulate genes involved in amino acid synthesis, transport, and charging.

(A) Row-normalized heatmaps of Nanostring gene expression data are shown from 1) serum-deprived wild-type (WT) or *Tsc2*$^{-/-}$ MEFs treated (16 h) with vehicle (Veh) or rapamycin (20 nM, Rap) (n=2), 2) serum-deprived WT MEFs treated with insulin (500 nM, 16 h, Ins) following 30-min pretreatment with vehicle or rapamycin (20 nM) (n=2), and 3) WT and *Tsc2*$^{-/-}$ MEFs transfected with *Atf4* siRNAs or non-targeting controls (siCT) and serum-deprived for 16 h (n=3). Genes are grouped by functional category and ranked in order of most significantly decreased with ATF4 knockdown for each group. Heatmap values are provided in Source data 2, and effects on ATF4 protein levels and mTORC1 signaling for each condition are shown by immunoblot in Figure S2A.

(B,C) qPCR analysis of the indicated transcripts in WT and *Tsc2*$^{-/-}$ MEFs (B) or WT MEFs stimulated with insulin (C) and treated with vehicle or rapamycin as in (A). Expression relative to vehicle-treated, unstimulated WT cells is graphed as mean ± SEM from three independent experiments, each with 3 biological replicates (n=9).

(D,E) Representative immunoblots of cells treated as in (B,C), with biological duplicates shown for each condition.

(F) Row-normalized heatmaps of Nanostring gene expression data for transcripts in the functional groups from (A) found to be significantly ($p < 0.05$) induced in *eIF2*$\alpha^{A/A}$ MEFs treated with insulin (500 nM, 16h) following 30-min pretreatment with vehicle or rapamycin (20 nM) (n=2). Genes are ranked by category in order of most significantly increased with insulin for each group. The heatmap values are provided in Source data 2.

(G) Representative immunoblot of cells treated as in (F), with biological duplicates shown for each condition.

(H) Representative immunoblot of *eIF2*$\alpha^{A/A}$ MEFs transfected with siRNAs targeting *Atf4, Tsc2,* or non-targeting controls prior to serum-starvation for 16 h.

(I,J) Representative immunoblot of serum-deprived LNCaP cells treated with vehicle or rapamycin (20 nM, 16 h) (I) or *Atf4* siRNAs versus non-targeting controls (siCT) (J), with biological duplicates shown for each.

(K,L) qPCR analysis of the indicated transcripts in LNCaP cells serum-starved in the presence of vehicle or rapamycin (20 nM, 16 h) (K) or transfected with *ATF4* siRNAs or non-targeting controls (siCT) and serum-starved for 16 h (L). Expression relative to vehicle-treated cells is graphed as mean ± SEM from two independent experiments, with 3 biological replicates each (n=6).

*$p < .05$, **$p < .01$, ***$p < .001$, ns = not significant. One-way ANOVA with Holm-Sidak method for multiple comparisons was used to determine statistical significance for (B,C). Unpaired two-tailed t-test was used to determine statistical significance for (F, K, L). (L,D,E,G,H,I,J) are representative of at least two independent experiments.

previously that mTORC1 regulates ATF4 in a manner that is independent of eIF2α-S51 phosphorylation (Ben-Sahra et al., 2016), chronic activation of mTORC1 upon loss of TSC2 is known to cause a basal increase in ER stress and activation of the ISR (Ozcan et al., 2008). Therefore, we utilized MEFs with endogenous, homozygous knock-in of the

247 *eIF2α-S51A* mutation (*eIF2α*$^{A/A}$), which fail to induce ATF4 downstream of cellular stress
248 (Figure supplement 2B) (Scheuner et al., 2001). Consistent with mTORC1-dependent,
249 ISR-independent regulation, insulin increases ATF4 protein levels and expression of its
250 gene targets involved in amino acid synthesis and one-carbon metabolism, amino acid
251 transporters, and amino-acyl tRNA synthetases in a rapamycin sensitive manner in these
252 cells, as shown by nanostring analysis and confirmed for a subset of genes by qPCR
253 (Figure 1F-G—figure supplement 2D). Notably, like insulin stimulation, genetic activation
254 of mTORC1 via siRNA-mediated knockdown of *Tsc2* in the *eIF2α*$^{A/A}$ MEFs also increased
255 ATF4 protein levels, further confirming that this regulation occurs independent of the ISR
256 (Figure 1H). Growth factor-independent activation of mTORC1 also occurs upon loss of
257 the PTEN tumor suppressor, and rapamycin was found to decrease protein levels and
258 ATF4-dependent expression of representative gene targets in established PTEN-
259 deficient prostate cancer cells, LNCaP and PC3 (Figure 2I-L—figure supplement 2E-H).
260 MYC has previously been shown to regulate the expression of many tRNA synthetase
261 genes and can be activated downstream of mTORC1 in some settings (Csibi et al., 2014;
262 Wall et al., 2008; Zirin et al., 2019). However, siRNA-mediated knockdown of c-MYC
263 failed to reduce expression of tRNA synthetase genes in *Tsc2*$^{-/-}$ MEFs, which were
264 suppressed by parallel knockdown of ATF4 (Figure 2—figure supplement 2I-J).

265 To determine whether ATF4 activation is both necessary and sufficient for mTORC1-
266 mediated regulation of gene targets related to amino acid acquisition and utilization, we
267 knocked out *Atf4* using CRISPR/Cas9 in *Tsc2*$^{-/-}$ MEFs and confirmed biallelic disruption
268 (Figure 3A). Protein levels of ATF4 targets were decreased in *Tsc2*$^{-/-}$ *Atf4*$^{-/-}$ MEFs and
269 fully rescued with expression of wild-type ATF4 but not a DNA-binding domain mutant
270 (ATF4^{DBD}) (Figure 3B). As mTORC1 regulates ATF4 translation through a mechanism
271 requiring its 5'-UTR (Ben-Sahra et al., 2016; Park et al., 2017), the stably rescued cell
272 lines, which express an ATF4 cDNA lacking the 5' UTR, exhibit protein expression of
273 ATF4 and its target MTHDF2 that are resistant to rapamycin (Figure 3C). The expression
274 of select ATF4 target transcripts were markedly decreased in *Tsc2*$^{-/-}$ *Atf4*$^{-/-}$ MEFs to a
275 similar extent to that measured in wild-type cells treated with rapamycin (Figure 3D).
276 These transcript levels were rescued with the expression of wild-type ATF4, but not

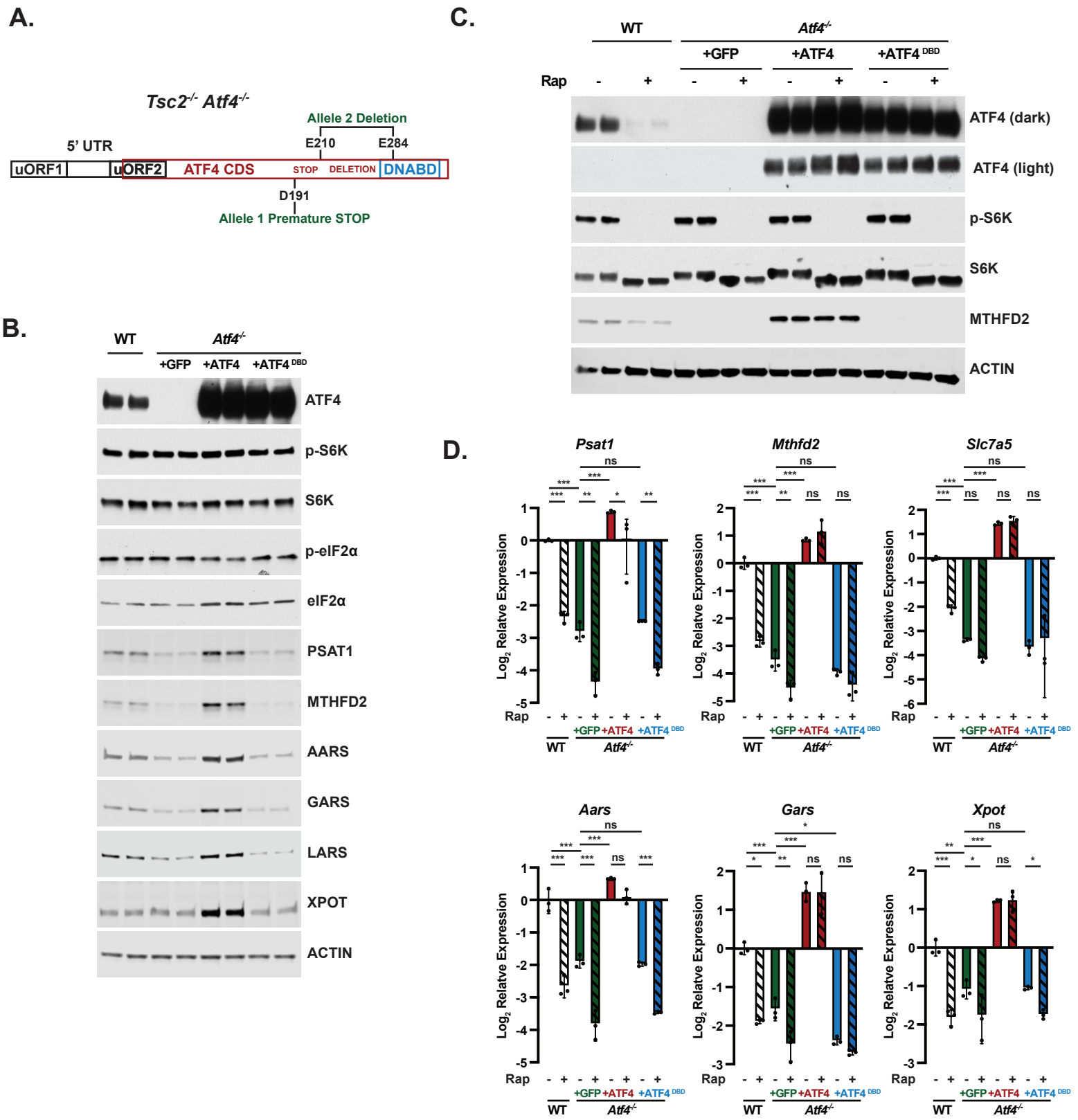

Figure 3. Use of ATF4 knockout cells and a rapamycin-resistant ATF4 to validate ATF4 targets regulated by mTORC1 signaling.
(A) Schematic of ATF4 transcript, including upstream open reading frames (uORFs), coding sequence (CDS), and DNA-binding domain (DNABD), highlighting location of CRISPRn guides biallelic location of ATF4 mutations generated in *Tsc2*$^{-/-}$ MEFs.

282 (B,C) Representative immunoblots of serum-deprived *Tsc2*$^{-/-}$ (WT) MEFs or *Tsc2*$^{-/-}$ *Atf4*$^{-/-}$
283 MEFs with stable expression of cDNAs encoding GFP, ATF4 lacking its 5'UTR, or a
284 DNABD mutant (DBD) of this ATF4 left untreated (B) or treated with vehicle or rapamycin
285 (20 nM, 16h) (C), with biological duplicates shown for each condition.
286 (D) qPCR analysis of the indicated transcripts from cells treated as in (C). Expression
287 relative to WT vehicle-treated cells is graphed as the $\log_2$ mean ± SD from a
288 representative experiment with three biological replicates (n=3). *p < 0.05, **p < 0.01, ***p
289 < 0.001, ns = not significant, calcuated via one-way ANOVA with Holm-Sidak method for
290 multiple comparisons.
291 (B-D) are representative of at least two independent experiments.

292 ATF4^{DBD}, in a manner that was completely or partially rapamycin resistant (Figure 3D).
293 These collective data show that mTORC1 signaling drives the expression of genes
294 involved in tRNA export and charging, amino acid uptake, and non-essential amino acid
295 synthesis through its downstream regulation of the ATF4 transcription factor.

296 **Activation of ATF4 contributes to the induction of protein synthesis downstream**
297 **of mTORC1**

298 mTORC1 induces protein synthesis through multiple downstream targets (Valvezan &
299 Manning, 2019). Given that the major mTORC1-regulated ATF4 target genes identified
300 above are involved in amino acid uptake, synthesis, and tRNA charging, we hypothesized
301 that ATF4 induction through mTORC1 signaling might contribute to the canonical
302 increase in protein synthesis upon mTORC1 activation. Relative rates of protein synthesis
303 were measured via [^{35}S]-methionine incorporation into newly synthesized proteins in
304 *Tsc2*$^{+/+}$ and *Tsc2*$^{-/-}$ cells treated with control siRNAs or *Tsc2*$^{-/-}$ cells treated with siRNAs
305 targeting ATF4 or Rheb, the small GTPase target of TSC2 that is an essential upstream
306 activator of mTORC1. As expected, siRNA-mediated knockdown of either ATF4 or Rheb
307 substantially decreased ATF4 protein levels in *Tsc2*$^{-/-}$ cells (Figure 4A). Importantly, the
308 elevated rate of protein synthesis in *Tsc2*$^{-/-}$ MEFs was decreased with ATF4 knockdown
309 to a similar extent to that observed with Rheb knockdown (Figure 4A,B). No change in
310 mTORC1 signaling or phosphorylation of eIF2α was observed with ATF4 knockdown in
311 this setting (Figure 4A—figure supplement 3). In addition, rapamycin treatment and ATF4
312 knockout reduced the rate of protein synthesis to a similar extent, however rapamycin

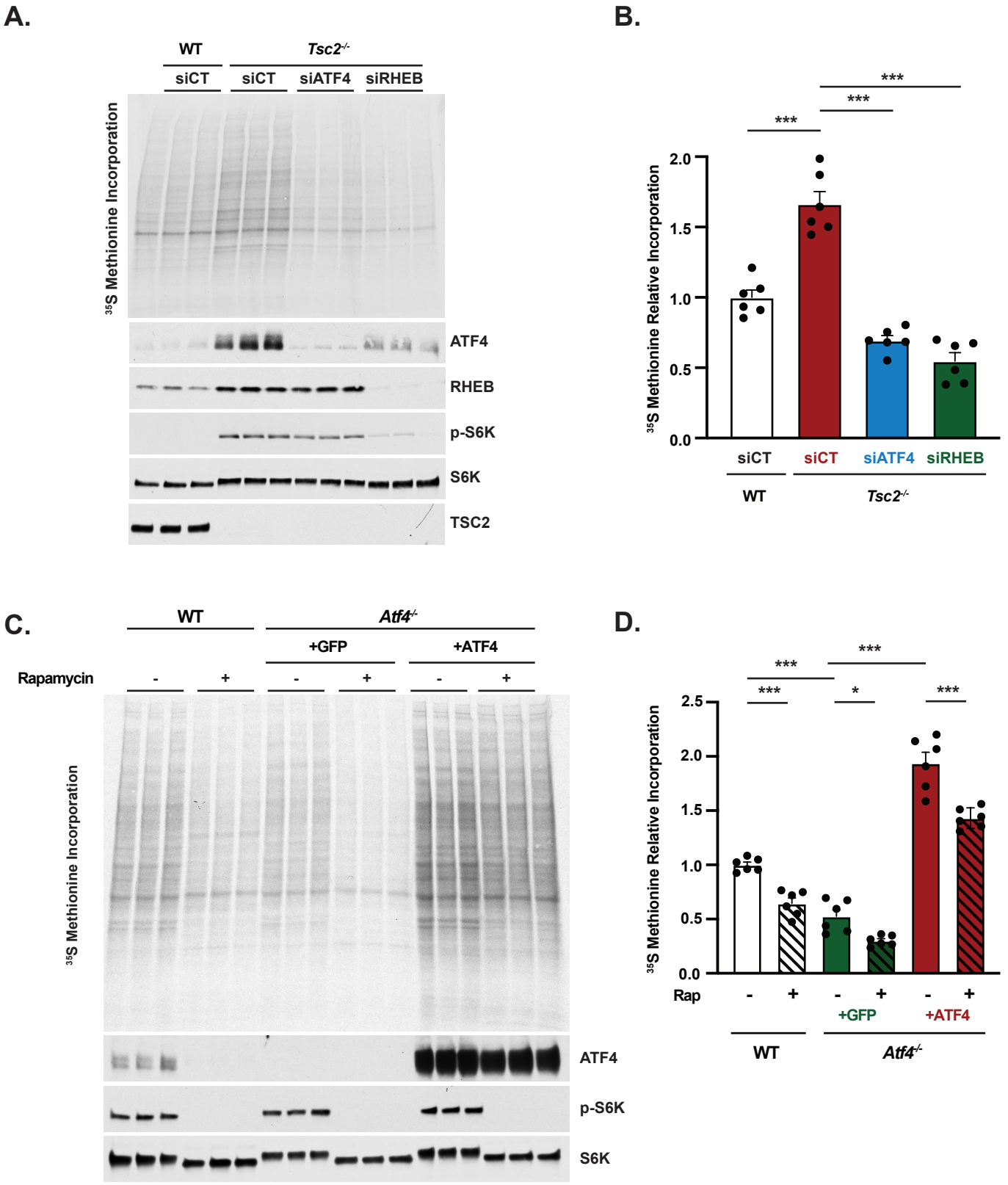

Figure 4. Activation of ATF4 contributes to the induction of protein synthesis downstream of mTORC1.

(A, B) Representative autoradiogram and immunoblot of WT and *Tsc2*$^{-/-}$ MEFs transfected with siRNAs targeting *Atf4* or *Rheb1* and *Rhebl1* or non-targeting controls (siCT) and serum-deprived for 16 h with a pulse label of [^{35}S]-methionine for the final 20 min (A) and quantified in (B). Biological triplicates from a representative experiment are shown in (A).

(B) is graphed as mean ± SEM from two independent experiments, each with 3 biological replicates (n=6).
(C,D) Representative autoradiogram and immunoblot of serum-deprived *Tsc2*$^{-/-}$ MEFs (WT) or *Tsc2*$^{-/-}$ *Atf4*$^{-/-}$ MEFs with stable expression of cDNAs encoding GFP or ATF4 lacking its 5'UTR treated with vehicle or rapamycin (20 nM, 16 h) with a pulse label of [^{35}S]-methionine for the final 20 min (C) and quantified in (D). Biological triplicates from a representative experiment are shown in (C). (D) is graphed as mean ± SEM from two independent experiments, each with 3 biological replicates (n=6).
(B,D) *$p < 0.05$, **$p < 0.01$, ***$p < 0.001$, ns = not significant, calculated via one-way ANOVA with Holm-Sidak method for multiple comparisons.

treatment further reduced protein synthesis in *Atf4* knockout cells (Figure 4C,D). Importantly, cells reconstituted with the rapamycin-resistant ATF4 cDNA exhibited rescued protein synthesis, surpassing that observed in cells with endogenous ATF4, but this enhanced protein synthesis was still significantly reduced with rapamycin. Together, these data suggest that ATF4 induction downstream of mTORC1 is necessary but not sufficient for mTORC1-regulated protein synthesis, consistent with the multiple mechanisms through which mTORC1 controls this key anabolic process.

mTORC1 regulates cystine uptake through ATF4

Among the 61 shared mTORC1- and ISR-induced ATF4 gene targets identified, the cystine-glutamate antiporter *Slc7a11* (xCT) was the most significantly induced gene upon insulin treatment (Figure 1F). SLC7A11 (also known as xCT) associates with SLC3A2 (CD98) at the plasma membrane and serves as the primary transporter of cystine, the oxidized form of cysteine and predominant cysteine species in both plasma and cell culture media, whereas reduced cysteine is transported through neutral amino acid systems (Figure 5A) (Bannai & Kitamura, 1980). Transcript levels of *Slc7a11* were sensitive to rapamycin in *Tsc2*$^{-/-}$ MEFs and dramatically decreased with ATF4 knockout (Figure 5B). Upon reconstitution with rapamycin-resistant ATF4, expression of *Slc7a11* was rescued and no longer sensitive to rapamycin, while the ATF4^{DBD} mutant was unable to restore *Slc7a11* transcript levels. A similar pattern of mTORC1- and ATF4-regulated expression was measured for *Slc3a2* (Figure 5C). *SLC7A11* transcript levels were also decreased with rapamycin and ATF4 knockdown in the PTEN-deficient cancer cell lines

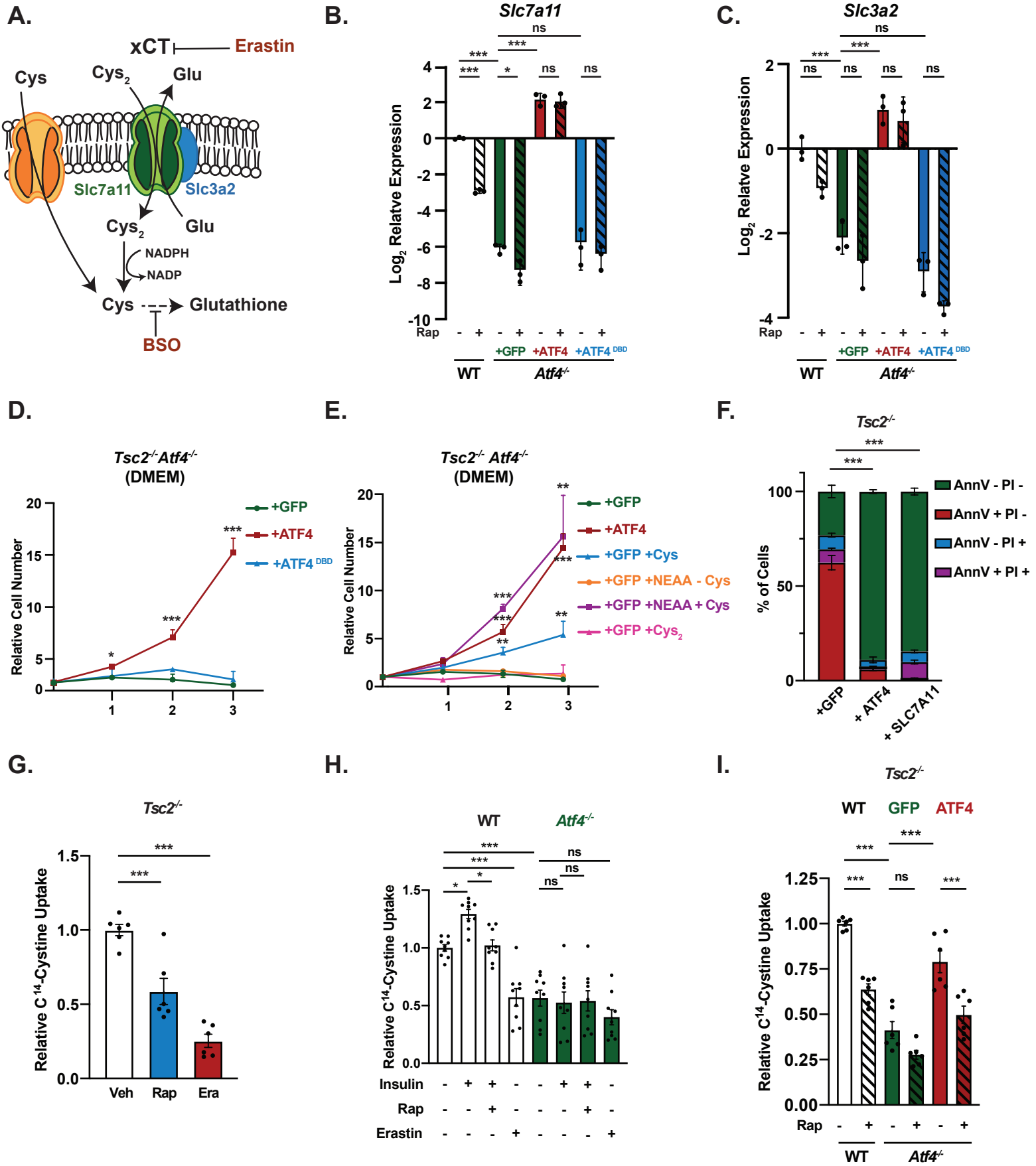

Figure 5. mTORC1 regulates cystine uptake through ATF4 and its target SLC7A11. (A) Schematic of transporter xCT, encoded by *Slc7a11*, which heterodimerizes with SLC3A2 to serve as a cystine (Cys_2)/glutamate anti-porter. Cystine is reduced to cysteine,

353 which is essential for glutathione synthesis. Cysteine transport is mediated by neutral
354 amino acid trasporters distict from xCT. The targets of Erastin and BSO, two compounds
355 used in this study, are also depicted.
356 (B,C) qPCR analysis of *Slc7a11* (B) or *Slc3a2* (C) in serum-deprived *Tsc2*$^{-/-}$ MEFs (WT)
357 and *Tsc2*$^{-/-}$ *Atf4*$^{-/-}$ MEFs with stable expression of cDNAs encoding GFP, ATF4 lacking its
358 5'UTR, or a DNABD mutant (DBD) of this ATF4 treated with vehicle or rapamycin (20 nM,
359 16 h). Expression relative to WT vehicle-treated cells is graphed as the $\log_2$ mean ± SD
360 from a representative experiment with three biological replicates (n=3).
361 (D, E) Representative growth curves of *Tsc2*$^{-/-}$ *Atf4*$^{-/-}$ MEFs with stable expression of GFP,
362 ATF4, or ATF4^{DBD} grown in 10% dialyzed FBS with DMEM (D) or DMEM supplemented
363 with cysteine alone (Cys, 1 mM), non-essential amino acids (100 μM each) lacking
364 cysteine (NEAA-Cys), or nonessential amino acids plus either cysteine (1 mM,
365 NEAA+Cys), or cystine (0.5 mM, NEAA+Cys_2) (E). Mean cell numbers ± SD relative to
366 Day 0 are graphed from three biological replicates (n=3).
367 (F) Cell death of *Tsc2*$^{-/-}$ *Atf4*$^{-/-}$ MEFs with stable expression of cDNAs encoding GFP,
368 ATF4 or SLC7A11 cultured in DMEM with 10% dialyzed FBS was quantified by Annexin
369 V and PI staining after 72 h and graphed as the mean percentage of total cells ± SD from
370 three biological replicates (n=3).
371 (G) Cystine uptake in serum-deprived *Tsc2*$^{-/-}$ MEFs treated with vehicle, rapamycin (20
372 nM), or erastin (10 uM) for 16h is graphed as the mean ± SEM radiolabel incorporation
373 from C^{14}-cystine over the final 10 min relative to vehicle-treated cells from two
374 independent experiments, with three biological replicates each (n=6).
375 (H) Cystine uptake in serum-deprived WT and *Atf4*$^{-/-}$ MEFs pretreated 30 min with vehicle
376 or rapamycin (20 nM) prior to insulin stimulation (500 nM, 24 h) or treated with erastin
377 (10μM, 30') was assayed and graphed as in (G) relative to vehicle-treated WT cells with
378 data from three independent experiments, with three biological replicates each (n=9).
379 (I) Cystine uptake in serum-deprived *Tsc2*$^{-/-}$ MEFs (WT) and*Tsc2*$^{-/-}$ *Atf4*$^{-/-}$ MEFs with
380 stable expression of cDNAs encoding GFP or ATF4 treated with vehicle or rapamycin (20
381 nM) for 16 h was assayed and graphed as in (G) relative to vehicle-treated WT cells with
382 data from two independent experiments, with three biological replicates each (n=6).
383 (B-F) are representative of at least two independent experiments.
384 *$p < 0.05$, **$p < 0.01$, ***$p < 0.001$, ns = not significant, calculated in (B,C,F,G,H,I) via
385 one-way ANOVA with Holm-Sidak method for multiple comparisons and in (D,E) via
386 unpaired two tailed t-test. For (F), the sum of AnnexinV+/PI- , AnnexinV-/PI+, and
387 AnnexinV+/PI+ populations were used for comparisons to the AnnexinV-/P- population.

388 LNCaP and PC3, although *SLC7A11* expression was relatively more resistant to
389 rapamycin in PC3 cells (Figure 5—figure supplement 4A-B). These data confirm and
390 extend the findings from RNA-Seq and Nanostring analyses (Figure 1F, Figure 2A and
391 2F),and demonstrate that ATF4 is both necessary and sufficient for the mTORC1-
392 mediated induction of *Slc7a11* expression.

393 ATF4 is known to be important for the uptake and synthesis of non-essential amino acids
394 (NEAAs) (Harding et al., 2003). In agreement with this, we observed that *Tsc2*$^{-/-}$ *Atf4*$^{-/-}$
395 cells fail to proliferate in DMEM, which only contains a subset of NEAAs, while addback
396 of wild-type ATF4, but not ATF4^{DBD}, restored proliferation (Figure 5D). Supplementation
397 of DMEM with a mixture of all NEAAs, including cysteine, allowed the *Tsc2*$^{-/-}$ *Atf4*$^{-/-}$ MEFs
398 to proliferate at the same rate as the ATF4-reconstituted cells, while NEAAs lacking
399 cysteine completely failed to support proliferation of these cells (Figure 5E). Furthermore,
400 supplementation with excess reduced cysteine alone, but not equimolar concentrations
401 of oxidized cysteine in the form of cystine, was able to significantly increase proliferation
402 of the *Tsc2*$^{-/-}$ *Atf4*$^{-/-}$ MEFs, albeit to a lesser extent than NEAAs plus cysteine. The majority
403 of these cells die after 72 hours in DMEM, and exogenous expression of either ATF4 or
404 SLC7A11 restores their survival (Figure 5F). Taken together, these data indicate that
405 defects in the acquisition of cysteine, which normally occurs through SLC7A11-mediated
406 uptake of cystine, underlie the inability of these cells to proliferate or survive in DMEM
407 and suggest a key role for mTORC1 signaling in controlling cystine uptake through ATF4.

408 To analyze the role of mTORC1 in cystine uptake, we employed both genetic (*Tsc2* loss)
409 and physiologic (insulin stimulation) activation of mTORC1, measuring [^{14}C]-cystine
410 uptake with or without rapamycin treatment or the xCT inhibitor erastin (Figure 5A) (Yang
411 & Stockwell, 2008). Both rapamycin and erastin significantly decreased [^{14}C]-cystine
412 uptake into *Tsc2*$^{-/-}$ MEFs (Figure 5G). In wild-type MEFs, insulin stimulated an increase
413 in cystine uptake that was inhibited with rapamycin, and this mTORC1-mediated
414 regulation of cystine transport was completely lost with ATF4 knockout (Figure 5H).
415 Additionally, *Tsc2*$^{-/-}$ *Atf4*$^{-/-}$ MEFs showed a decrease in cystine uptake when compared to
416 parental *Tsc2*$^{-/-}$ MEFs, which could be rescued with re-expression of ATF4. Surprisingly,
417 cystine consumption in cells reconstituted with rapamycin-resistant ATF4 was still
418 significantly sensitive to rapamycin treatment, suggesting the existence of additional,
419 ATF4-independent mechanisms influencing the transport or cellular incorporation of
420 cystine downstream of mTORC1. Thus, mTORC1 promotes cystine uptake to support cell
421 proliferation and survival, at least in part, through the activation of ATF4 and induction of
422 *Slc7a11* expression.

423 **mTORC1 regulates glutathione levels through ATF4-mediated induction of *Slc7a11***

424 Cysteine, generally acquired through cystine uptake and reduction, is an essential
425 component of the tripeptide glutathione (Figure 5A), the most abundant antioxidant in
426 cells (Meister, 1983). We hypothesized that the regulation of cystine uptake through
427 mTORC1 and ATF4 might influence cellular glutathione content. Indeed, mTORC1
428 inhibition with rapamycin or Torin1 significantly decreased total glutathione levels in *Tsc2*$^{-}$
429 $^{/-}$ MEFs, albeit less than buthionine-sulfoximine (BSO), a direct inhibitor of glutathione
430 synthesis (Figure 6A) (Griffith & Meister, 1979). Similar to BSO treatment, mTOR
431 inhibitors decreased both reduced (GSH) and oxidized (GSSG) glutathione levels to the
432 same degree, indicating effects on total glutathione abundance rather than redox state
433 (Figure supplement 5A). Stable reconstitution of *Tsc2*$^{-/-}$ MEFs with TSC2 also decreased
434 total glutathione levels (Figure 6B). To examine this response *in vivo*, we employed a
435 mouse model of tuberous sclerosis complex involving xenograft tumors derived from the
436 rat *TSC2-/-* tumor cell line ELT3 (Hodges et al., 2002). To avoid major differences in tumor
437 size from the treatments, we treated tumor-bearing mice for just 5 days with either vehicle
438 or rapamycin, prior to harvesting tumors for immunoblot analysis and metabolite profiling.
439 Importantly, we found that rapamycin treatment strongly decreased ATF4 protein levels
440 in these tumors with a concomitant decrease in glutathione levels, measured by LC-MS
441 in tumor metabolite extracts (Figure 6C-D). An analysis of published metabolomics data
442 (Tang et al., 2019) also revealed that rapamycin treatment significantly decreased
443 glutathione levels in human TSC2-deficient angiomyolipoma cells (Figure 6—figure
444 supplement 5B). Likewise, inhibition of mTORC1 signaling with rapamycin or Torin1 in
445 the PTEN-deficient LNCaP and PC3 cell lines resulted in a significant decrease in total
446 glutathione levels, although the degree of decrease varied between the two cell lines,
447 perhaps reflecting their differences in the response of *SLC7A11* transcript levels to
448 rapamycin (Figure 6E—supplemental figure 4A-B).

449 To determine the role of ATF4 and SLC7A11-dependent cystine uptake in glutathione
450 synthesis downstream of mTORC1 signaling, we compared *Tsc2*$^{-/-}$ MEFs with or without

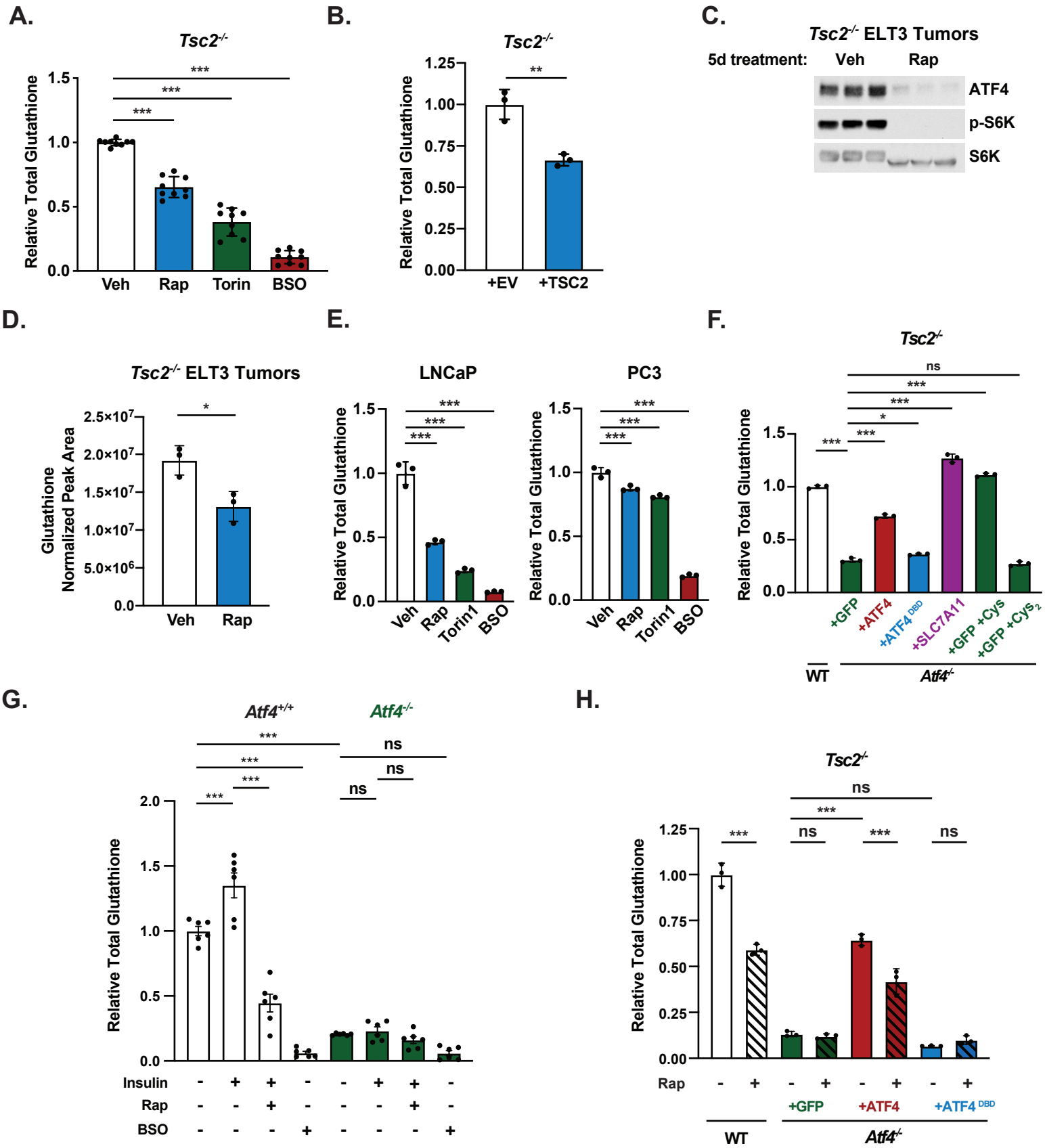

Figure 6. mTORC1 regulates cellular glutathione levels through ATF4 and SLC7A11-mediated cystine uptake.

(A) Total glutathione in serum-deprived *Tsc2*$^{-/-}$ MEFs treated with rapamycin (20 nM), Torin1 (250 nM), or BSO (10 μM) for 16 h is graphed as mean ± SEM relative to vehicle-treated cells from three independent experiments, each with three biological replicates

456 (n=9). Relative abundance of reduced (GSH) and oxidized (GSSG) glutathione from this
457 experiment is shown in Figures S5A.
458 (B) Relative total glutathione in serum-deprived *Tsc2*$^{-/-}$ MEFs with stable expression of a
459 cDNA encoding TSC2 or empty vector (EV) control is graphed as mean ± SD from a
460 representative experiment with three biological replicates (n=3).
461 (C, D) Immunoblot (C) and relative glutathione levels measured by LC-MS/MS (D) from
462 *Tsc2*$^{-/-}$ ELT3 xenograft tumors resected from mice treated for 5 days with vehicle or
463 rapamycin (1 mg/kg on days 1, 3, and 5) (n = 3 mice/group). Glutathione levels from
464 rapamycin-treated human *TSC2*$^{-/-}$ tumor cells are shown in Figure S5B.
465 (E) Total glutathione in serum-deprived LNCaP (left) and PC3 (right) cells treated with
466 vehicle, rapamycin (20 nM), Torin1 (250 nM), or BSO (50 μM) for 24 h is graphed as
467 mean ± SD relative to vehicle treated cells from a representative experiment with three
468 biological replicates (n=3).
469 (F) Total glutathione in serum-deprived *Tsc2*$^{-/-}$ MEFs (WT) and *Tsc2*$^{-/-}$ *Atf4*$^{-/-}$ MEFs with
470 stable expression of cDNAs encoding GFP, ATF4, ATF4^{DBD}, or SLC7A11 grown in DMEM
471 and supplemented, where indicated, with cysteine (1 mM) or cystine (0.5 mM) is graphed
472 as mean ± SD relative to WT cells from a representative experiment with three biological
473 replicates (n=3). Relative glutathione in these cells supplemented with NEAA with or
474 without Cys, measured by LC-MS/MS, is shown in Figure S5C.
475 (G) Total glutathione in serum-deprived *Atf4*$^{+/+}$ and *Atf4*$^{-/-}$ MEFs pretreated 30 min with
476 vehicle or rapamycin (20 nM) prior to insulin stimulation (500 nM, 24 h) or treated with
477 BSO (10μM, 24 h) is graphed as mean ± SEM relative to unstimulated Atf4$^{+/+}$ cells from
478 two independent experiments, with 3 biological replicates each (n=6).
479 (H) Total glutathione in serum-deprived *Tsc2*$^{-/-}$ MEFs (WT) and *Tsc2*$^{-/-}$ *Atf4*$^{-/-}$ MEFs with
480 with stable expression of cDNAs encoding GFP, ATF4 lacking its 5'UTR, or a DNABD
481 mutant (DBD) of this ATF4 treated with vehicle or rapamycin (20 nM) for 16 h is graphed
482 as mean ± SD relative to vehicle-treated WT cells from a representative experiment with
483 three biological replicates (n=3). Rapamycin-sensitive, ATF4-independent expression of
484 glutathione synthesis genes is shown in Figures S5D and E.
485 (B, E, F, H) are representative of at least two independent experiments. *p < .05, **p <
486 .01, ***p < .001, ns = not significant, calculated in (A,E,F,G,H) via one-way ANOVA with
487 Holm-Sidak method for multiple comparisons and in (B,D) via unpaired two tailed t-test.

488 *Atf4* knockout. Total glutathione levels were significantly decreased in the *Tsc2*$^{-/-}$ *Atf4*$^{-/-}$
489 MEFs, and exogenous expression of ATF4 or SLC7A11, but not ATF4^{DBD}, was able to
490 restore glutathione levels (Figure 6F). Supplementation with all NEAAs or just cysteine,
491 transported through neutral amino acid systems, but not equimolar concentrations of
492 cystine, transported through SLC7A11, also rescued total glutathione levels, as measured
493 by either enzymatic assay or LC-MS (Figure 6F—figure supplement 5C). Furthermore,
494 insulin also stimulated an increase in glutathione levels in a manner sensitive to
495 rapamycin, which was not observed in *Atf4* knockout cells (Figure 6G). Likewise, the
496 rapamycin-sensitive nature of glutathione in *Tsc2*$^{-/-}$ MEFs was completely lost in *Tsc2*$^{-/-}$

497 *Atf4*$^{-/-}$ MEFs (Figure 6H). Glutathione levels were restored to these cells upon exogenous
498 expression of ATF4, but not the ATF4^{DBD} mutant. However, glutathione was still
499 significantly reduced with rapamycin treatment in cells expressing the rapamycin-
500 resistant ATF4, suggesting additional ATF4-independent mechanisms contributing to this
501 regulation (Lam et al., 2017). Indeed, we found that expression of both the catalytic
502 (GCLC) and regulatory (GCLM) subunits of glutamate-cysteine ligase, the first enzyme of
503 glutathione synthesis, was sensitive rapamycin, in an ATF4-independent manner (Figure
504 6—figure supplement 5D-E). Together, these data show that mTORC1 signaling induces
505 glutathione synthesis, at least in part, through the activation of ATF4 and SLC7A11-
506 dependent cystine uptake.

507 **Discussion**

508 Our findings expand the functional repertoire of mTORC1 signaling as it relates to the
509 control of anabolic processes and cellular metabolism through its noncanonical activation
510 of ATF4. Importantly, less than 10% of stress-responsive, ATF4-dependent targets were
511 found to be significantly stimulated through the mTORC1-mediated activation of ATF4 in
512 response to insulin. Among others, we found that genes involved in amino acid
513 biosynthesis, transport, and tRNA charging were induced by mTORC1-ATF4 signaling,
514 many to a comparable level to that of ER stress induction with tunicamycin. While the
515 molecular nature of this selective induction is unknown, it is possible that the 61 ATF4-
516 depenent genes shared between mTORC1 signaling and the ISR represent the most
517 high-affinity gene targets of ATF4. Since mTORC1 signaling leads to a more modest
518 increase in ATF4 protein levels than does the ISR, the selective induction of these genes
519 might be reminiscent of the dose-dependent activation of MYC target genes documented
520 in other studies (Sabò et al., 2014; Schuhmacher & Eick, 2013; Walz et al., 2014).
521 Alternatively, as a basic helix loop helix transcription factor, ATF4 engages it's gene
522 targets as heterodimers with various binding partners, including C/EBPβ and CHOP
523 (Cohen et al., 2015; Ebert et al., 2020; Gachon et al., 2001; Newman & Keating, 2003;
524 Vallejo et al., 1993) which could be more narrowly regulated by mTORC1 signaling than
525 by the ISR.

526 Consistent with the specific ATF4 target genes induced by mTORC1 signaling, including
527 those involved in amino acid acquisition and tRNA charging, we found that ATF4
528 activation contributes to both canonical (e.g., protein synthesis) and new (e.g., glutathione
529 synthesis) functions of mTORC1. As mTORC1 stimulates protein synthesis through
530 multiple downstream targets (Holz et al., 2005; Jefferies et al., 1994; Ma & Blenis, 2009;
531 Raught et al., 2004; Thoreen et al., 2012), it was not surprising to find that ATF4 was
532 necessary but not sufficient for the increased rate of protein synthesis accompanying
533 mTORC1 activation. We also demonstrate that mTORC1 signaling regulates the
534 abundance of total cellular glutathione, both reduced and oxidized, at least in part through
535 the ATF4-dependent induction of the cystine transporter SLC7A11, a major source of the
536 cysteine that is limiting for glutathione synthesis. Importantly, this mTORC1-ATF4-
537 mediated transcriptional up-regulation of SLC7A11 leading to increased cystine uptake
538 temporally follows the inhibition of SLC7A11 recently found to be mediated through
539 mTORC2 and Akt-dependent transient phosphorylation of the transporter (Gu et al., 2017;
540 Lien et al., 2017). Our findings are consistent with a recent study indicating rapamycin-
541 sensitive expression of xCT in TSC models, which the authors attribute to the OCT1
542 transcription factor (Li et al., 2019). However, our study indicates that the mTORC1-
543 mediated activation of ATF4 is both necessary and sufficient for this regulation. The
544 transcription factor NRF2 (also known as NFE2L2) is activated by oxidative stress and is
545 a master regulator of the enzymes required for glutathione synthesis, as well as SLC7A11
546 to increase cystine uptake (Habib et al., 2015; Sasaki et al., 2002; Ye et al., 2014). While
547 NRF2 depletion can decrease the viability of cells with TSC gene loss (Zarei et al., 2019),
548 we have no evidence from this or previous studies that mTORC1 signaling influences the
549 levels or activity of NRF2 (Zhang et al., 2014).

550 mTORC1 serves to couple growth signals to the coordinated control of anabolic
551 processes, including the biosynthesis of protein, lipids, and nucleotides, as well as
552 metabolic pathways that support this anabolic state (Valvezan & Manning, 2019). This
553 metabolic program is orchestrated to provide biosynthetic precursors and directly promote
554 the synthesis of macromolecules while also maintaining cellular homeostasis and

555 preventing nutrient or metabolic stress. For example, mTORC1 signaling promotes
556 metabolic flux through the NADPH-producing oxidative branch of the pentose phosphate
557 pathway, thereby providing the reducing power essential to support an mTORC1-
558 stimulated increase in *de novo* lipid synthesis (Duvel et al., 2010). Importantly, NADPH is
559 also essential to reduce cystine, taken up through SLC7A11, into to molecules of cysteine
560 for use in glutathione synthesis, in addition to being required to regenerate reduced
561 glutathione following its oxidation. Supporting this logic of a coordinated metabolic
562 program downstream of mTORC1, pro-growth signaling through mTORC1 likely
563 promotes glutathione synthesis to help buffer against the oxidative stress that
564 accompanies anabolic metabolism and increased rates of protein synthesis (Han et al.,
565 2013; Harding et al., 2003; Kong & Chandel, 2018).

566 Our findings add ATF4 to SREBP and HIF1, as nutrient- and stress-sensing transcription
567 factors that are independently co-opted by mTORC1 signaling to drive the expression of
568 metabolic enzymes and nutrient transporters. Unlike adaptive signals stemming from the
569 depletion of individual nutrients, such as amino acids, sterols, or oxygen, pro-growth
570 signals through mTORC1 can activate these transcription factors together to support a
571 broader anabolic program. It will be important in future studies to understand the dual
572 regulation of these transcription factors by both pro-growth and adaptive mechanisms as
573 it relates to settings of physiological (fasting and feeding) and pathological (tumor
574 development) nutrient fluctuations.

575 **Materials and Methods**

576 **Cell culture**

577 MEFs and PC3 cells were maintained in Dulbecco's Modified Eagle's Medium (DMEM;
578 Corning/Cellgro, 10-017-CV) with 10% fetal bovine serum (FBS, Corning/Gibco). LNCaP
579 cells were maintained in RPMI-1640 (Corning/Cellgro 10-040-CV) with 10% FBS. *Tsc2*$^{-/-}$
580 (*p53*$^{-/-}$) MEFs and littermate derived wildtype counterparts were provided by David
581 Kwiatkowski (Brigham and Women's Hospital, Boston MA). *eIF2*$\alpha^{S/S}$ (WT) and *eIF2*$\alpha^{A/A}$
582 (S51A knock-in mutant) MEFs were provided by Randal Kaufman (Sanford-Burnham-

583 Prebys Medical Discovery Institute, La Jolla CA) and were not used above passage 3
584 (after received). Cancer cell lines were obtained from ATCC. Atf4$^{-/-}$ MEF lines generated
585 in this study were maintained in Dulbecco's Modified Eagle's Medium (DMEM;
586 Corning/Cellgro, 10-017-CV) with 10% FBS, 55 μM 2-mercaptoethanol (Thermo,
587 21985023), and 1X MEM nonessential amino acid mix (final concentration 100 μM of
588 alanine, aspartate, asparagine, glutamate, glycine, proline, and serine, Thermo
589 11140050). In experiments with supplementation of excess cysteine, cells were plated in
590 DMEM with 10% FBS, 1 mM cysteine, and 1X MEM nonessential amino acid mix.

591 **siRNA knockdowns**

592 Cells were transfected with 20 nM of the indicated siRNAs using Opti-MEM (Thermo,
593 31985062) and RNAimax (Thermo, 13778150) according to the manufacturer's protocol.
594 siRNAs were from GE Life Sciences/Dharmacon: Non-targeting Pool (D-001810-10-50),
595 *Myc* (L-040813-00-0010), *Atf4* (mouse, L-042737-01-0020), *Rheb* (L-057044-00-0020),
596 *RhebL1* (L-056074-01-0020), *Tsc2* (L-047050-00-0020), and *ATF4* (human, L-005125-
597 00-0020). 48 h post-transfection, cells were serum starved overnight prior to lysis for
598 immunoblotting, RNA extraction, or protein synthesis assays. For protein synthesis
599 assays, transfection of siRNAs was performed a second time 24 h after the first
600 transfection, which was necessary to achieve sufficient knockdown of Rheb to reduce
601 mTORC1 activity.

602 **Generation and validation of *Atf4*$^{-/-}$ and reconstituted cell lines**

603 *Tsc2*$^{+/+}$ (WT) and *Tsc2*$^{-/-}$ MEFs lacking Atf4 were generated by CRISPR-Cas9 mediated
604 deletion using pSpCas9n(BB)-2A-GFP (PX461) vector (Addgene, 48140) according to
605 the previously described protocol (Ran et al., 2013). The paired nickase guides were
606 designed using E-CRISP (Heigwer et al., 2014) and targeted the sequences
607 AGCATAGCCCCTCCACCTCC and GACAATCTGCCTTCTCCAGG in Exon 2 of ATF4.
608 48 h post-transfection, single GFP-positive cells were sorted into 96-well plates. Cells
609 were cultured in DMEM with 10% FBS supplemented 1X MEM nonessential amino acids
610 and 55 μM 2-mercaptoethanol. Single cell clones were grown for immunoblot analysis
611 and those showing loss of ATF4 protein were selected for sequence analysis involving

612 the isolation of genomic DNA (Qiagen, 69504), PCR amplification using KOD Xtreme™
613 Hot Start DNA Polymerase (Millipore, 71975) and primers TCGATGCTCTGTTTCGAATG
614 and CTTCTTCCCCCTTGCCTTAC flanking the targeted deletion site, and sequencing on
615 an ABI3730xl DNA analyzer at the DNA Resource Core of Dana-Farber/Harvard Cancer
616 Center (funded in part by NCI Cancer Center support grant 2P30CA006516-48). The
617 mutations were identified using CRISP-ID software (Dehairs et al., 2016). For the final
618 clones selected, the mutations generated in the *Tsc2*$^{+/+}$ MEFs include an out-of-frame 17-
619 base pair deletion starting at the codon encoding T237, resulting in a premature STOP
620 codon, and a large out-of-frame 73-base pair deletion starting after the codon encoding
621 G219, resulting in a premature STOP codon. The mutations generated in the *Tsc2*$^{-/-}$ MEFs
622 include an out-of-frame 245-base pair deletion starting at the codon encoding G190,
623 resulting in a premature STOP codon after the D191 codon, and an in-frame deletion
624 removing the sequences encoded between E210 and E284.

625 For generation of *ATF4* rescue vectors, the *Atf4* cDNA was amplified from the plasmid
626 21845 from Addgene (Harding et al., 2000). Restriction enzyme cloning with AgeI and
627 ClaI was used to insert the ATF4-coding sequence (lacking the 5' and 3' UTR) into
628 pTRIPZ plasmid for doxycycline-inducible expression. The ATF4^{DBD} mutant, in which
629 amino acids 292-298 of the DNA-binding domain are changed from RYRQKKR to
630 GYLEAAA (He et al., 2001; Lange et al., 2008) was generated by DpnI-mediated site-
631 directed mutagenesis using KOD Xtreme™ Hot Start DNA Polymerase. The dox-
632 inducible pTRIPZ and SLC7A11 plasmids were a gift from Alex Toker (Beth Israel
633 Deaconess Medical Center). cDNA expression was induced with 1 μg/mL of doxycycline
634 (sigma-Aldrich, D3447) for 12-24 hrs before assays were conducted. GFP was inserted
635 into pTRIPZ to produce the control vector. Lentivirus was generated in HEK293T cells
636 transfected with pMD2.G and psPAX2 (Addgene, 12259 and 12260) and the given
637 pTRIPZ constructs. 48 h post-transfection the viral medium was used to infect the target
638 cells, which were selected with 8 μg/mL puromycin. TSC2 addback cell lines were
639 generated by retroviral infection following transfection of PT67 cells with pBabe hygro
640 IRES-EV or pBabe hygro IRES-TSC2. Cells were selected with 400 μg/mL hygromycin B
641 (Thermo, 10687010).

642 **RNA-sequencing**

643 Wild-type and *Atf4*$^{-/-}$ MEFs were grown to 70% confluence in 6 cm plates and were serum-
644 starved in the presence of 2-mercaptoethanol and 1X MEM NEAA mixture and treated
645 with vehicle (DMSO) or 20 nM rapamycin (LC Laboratories, R5000) for 30 min prior to
646 stimulation with vehicle (water) or 500 nM insulin (Alpha Diagnostic, INSL 16-N-5) for 16
647 h or treated with vehicle (DMSO) or 2 μg/mL tunicamycin (Sigma-Aldrich, T7765) for 4,
648 8 or 16 h. RNA was harvested with TRIzol according to the manufacturer's protocol
649 (Thermo, 15596018). All samples passed RNA quality control measured by NanoDrop
650 1000 Spectrophotometer (NanoDrop Technologies) and 2100 Bioanalyzer (Agilent
651 Technologies). cDNA libraries were generated to produce 150 base pair paired-end reads
652 on an Illumina NovaSeq with read depth of 20 million paired reads per sample. Reads
653 were aligned and annotated to the Ensembl *Mus musculus* GRCm38.p6 genome
654 assembly using the align and featureCounts functions from the Rsubread package (2.0.1)
655 in R (3.6.3) (Liao et al., 2019). Differential gene expression analysis was performed using
656 the voom and eBayes functions from the EgdeR (3.28.1) and Limma (3.42.2) packages,
657 respectively (Ritchie et al., 2015; Robinson et al., 2009). The enrichKEGG function from
658 the clusterProfiler package (3.14.3) was used to perform KEGG pathway over-
659 representation tests (Guangchuang Yu, 2012). Gene set enrichment analysis was
660 evaluated using GSEA software from the Broad Institute (Subramanian et al., 2005).
661 Computations were run on the FASRC Cannon cluster, supported by the Faculty of Arts
662 and Sciences Division of Science Research Computing Group at Harvard University.
663 Pseudogenes and unannotated genes were excluded from the Venn diagram shown in
664 Figure 1C. The source data can be found at GEO under the accession number
665 GSE158605.

666 **Immunoblotting**

667 Cells were lysed in ice-cold Triton lysis buffer (40mM HEPES pH 7.4, 120mM NaCl, 1mM
668 EDTA, 1% Triton X-100, 10mM sodium pyrophosphate, 10 mM glycerol 2-phosphate, 50
669 mM NaF, 0.5 mM sodium orthovanadate, 1 μM Microcystin-LR, and Sigma protease
670 inhibitor cocktail P8340). Samples were centrifuged at 20,000 x g for 10 min at 4°C and

671 protein concentration in the supernatant was determined by Bradford assay (Bio-Rad,
672 5000202) and normalized across samples. Proteins were separated by SDS-PAGE,
673 transferred to nitrocellulose membranes, and immunoblotted with indicated antibody.
674 Primary antibodies used: MTHFD2 (Protein Tech, 12270-1-AP), PSAT1 (Protein Tech
675 20180-1-AP), phospho (P)-S6K1 T389 (Cell Signaling Technologies (CST), 9234), ATF4
676 (CST, 11815), eIF2α (CST 9722), P-eIF2α S51 (CST, 9721), S6K1 (CST, 2708), AARS
677 (Bethyl Antibodies, A303-475A-M), GARS (Bethyl Antibodies, A304-746A-M) LARS
678 (Bethyl Antibodies, A304-316A-M), XPOT (Aviva Biotechnologies, ARP40711_P050),
679 TSC2 (CST, 4308), β-actin (Sigma-Aldrich, A5316); secondary antibodies used: IRDye
680 800CW Donkey anti-Mouse IgG (H + L) (LI-COR, 926-32212) and Donkey anti-Rabbit
681 IgG (H + L) (LI-COR, 925-32213), and HRP-conjugated anti-mouse and anti-rabbit
682 secondary antibodies from (CST, 7074 and 7076). Immunoblots of MTHFD2, PSAT1,
683 AARS, GARS, LARS, and XPOT were imaged using Odyssey CLx Imaging System (LI-
684 COR Biosciences). β-actin was developed with Odyssey CLx Imaging System or
685 enhanced chemiluminescence assay (ECL). All remaining immunoblots were developed
686 using ECL.

687 **NanoString analysis**

688 RNA was harvested using TRIzol from cells at 70% confluence. All samples passed RNA
689 quality control measured by NanoDrop 1000 Spectrophotometer. Parallel plates were
690 lysed for immunoblots. The isolated RNA was analyzed using a custom NanoString probe
691 library according to the manufacturer's instructions (NanoString Technologies). Briefly,
692 sample RNA was hybridized to RNA-probes at 65 °C for 16 h, excess probe was washed
693 away, and an nCounter SPRINT was used to quantify specific mRNA molecules present
694 in each sample. Direct mRNA counts were normalized to internal control genes and
695 mRNA expression was analyzed using nSOLVER software. Heatmaps were generated
696 with Morpheu software from the Broad Institute
697 (https://software.broadinstitute.org/morpheus). Transcripts with 100 counts or fewer, a
698 value based off of negative control samples, were not included in our analyses.

699 **qPCR**

700 For gene expression analysis, RNA was isolated with TRIzol according to the
701 manufacturer's protocol. All samples passed RNA quality control measured by NanoDrop
702 1000 Spectrophotometer. cDNA was generated with Superscript III First Strand Synthesis
703 System for RT-PCR (Thermo, 18080051). Quantitative RT-PCR was performed with a
704 CFX Connect Realtime PCR Detection System (Bio-Rad) using iTaq Universal SYBR
705 Green Supermix (Bio-Rad, 1725125). Samples were quantified by the ΔΔCT method,
706 normalized to *β-actin* (mouse samples) or *RPLP0* (human samples) to quantify relative
707 mRNA expression levels.

708 qPCR Primers:

Atf4	ATGGGTTCTCCAGCGACAAG	CCGGAAAAGGCATCCTCCTT
Psat1	GCTGTCGCCTTAGCACCA	TGGATCTCCAACAATACCGAGTG
Mthfd2	TCCTTGTTGTCTGCGTTGGC	CTTCATTTCGCACTGCCGCC
Slc7a5	GGACAAGGTGATGCGTCCAA	GCCAACACAATGTTCCCCAC
Aars	TTGCTATTCCCTCGGAGCAC	CTCCTCGGGAACCTTAGCTC
Gars	GGCAGAGGTCTCTGAGCTG	GCACGATGGTCATAAGCTGC
Cars	GAGCAGGCTGCCGACTACA	TATAGCTACGCGTGCTGAGG
Nars	GAGCCGGCCTGTGTAAAGAT	GACCCAGCCAAACACCTTCA
Iars	TATTGCATCACCTCCAGACGC	TGAACCATTCTGTTGCTGGGA
Gclc	TGTACTCCACCCTCGTCACCC	CTGCTGTCCCAAGGCTCG
Gclm	TGGGCACAGGTAAAACCCAA	CTGGGCTTCAATGTCAGGGA
Slc7a11	ATCTCCCCCAAGGGCATACT	GCATAGGACAGGGCTCCAAA
Slc3a2	TGATGAATGCACCCTTGTACTTG	GCTCCCCAGTGAAAGTGGA
Actin	CACTGTCGAGTCGCGTCC	TCATCCATGGCGAACTGGTG
PSAT1	AAAAACAATGGAGGTGCCGC	GGCTCCACTGGACAAACGTA
ASNS	TGGCTGCCTTTTATCAGGGG	TCTGCCACCTTTCTAGCAGC
MTHFD2	GGCAGTTCGAAATGAAGCTGTT	GCCAACCAGGATCACACTCA
SLC7A5	GACTACGCCTACATGCTGGA	AGCAGCAGCACGCAGAG
AARS	CCATTCAGAAGGGCACAGGT	TATCCACGCCCTGTGTTGTC
GARS	GCCAGCAGGGAGATCTTGTG	CCAGCTCCTTTGCTTCCAGA
XPOT	GACGCAGAGCGACTAGAGG	TAAACATCTTCCCTATCACTCCATC
SLC7A11	AAGGTGCCACTGTTCATCCC	ATGTTCTGGTTATTTTCTCCGACA
RPLP0	CCTCGTGGAAGTGACATCGT	ATCTGCTTGGAGCCCACATT

709 **Protein synthesis assay**

710 MEFs cultured in 6-well plates were serum starved in DMEM for 16 h. Cells were washed
711 twice with PBS and changed to methionine/cystine/glutamine-free DMEM (Thermo,
712 21013024) supplemented with 0.5 mM L-cystine (Sigma, 57579) and L-glutamine (4 mM)
713 with 50 μCi/mL ^{35}S-methionine (PerkinElmer, NEG009L005MC) for 20 min. Cells were
714 washed twice in ice cold PBS and lysed in ice-cold Triton lysis buffer. Total protein
715 concentrations were normalized following a Bradford assay, and samples were separated
716 by SDS-PAGE and transferred to nitrocellulose. ^{35}S-methionine incorporation into protein
717 was analyzed by autoradiography and abundance of specific proteins was determined by
718 immunoblot. Relative rates of protein synthesis were quantified using ImageJ Software
719 (NIH) to quantify radiolabeled protein per lane for each sample. For *Atf4*$^{-/-}$ cell lines,
720 exogenous cDNA expression was induced for 16 h with 150 ng/mL doxycycline. Cells
721 were serum-starved in the presence of doxycycline (150 ng/mL), 1X MEM NEAA mixture,
722 1 mM cysteine (Sigma, C7477), and vehicle (DMSO) or rapamycin (20 nM). Protein
723 synthesis was assayed with 20 min labeling in the absence of MEM NEAA and cysteine
724 to avoid competition of ^{35}S-methionine uptake with the supplemented amino acids.

725 **Proliferation assay**

726 To quantify cell proliferation, cells were plated in DMEM in 6-well plates in triplicate in the
727 presence of 2-mercaptoethanol, MEM NEAA mixture, 10% FBS, and doxycycline (1
728 μg/mL). 24 h after plating, cells were washed twice with PBS and media was changed to
729 DMEM with 10% dialyzed FBS, doxycycline (1 μg/mL), and the amino acid supplements
730 indicated for each experiment, with media refreshed daily. Starting on day 0, viable cells
731 from triplicate wells corresponding to each condition or cell line were counted using a
732 hemocytometer, excluding dead cells detected by trypan blue stain (Sigma-Aldrich,
733 T8154).

734 **Analysis of cell death**

735 Cells were plated in DMEM in 6-well plates in triplicate in the presence of 2-
736 mercaptoethanol, MEM NEAA mixture, 10% FBS, and doxycycline (1 μg/mL). 24 h after
737 plating, cells were washed twice with PBS and media was changed to DMEM with 10%

738 dialyzed FBS and doxycycline (1 μg/mL). 72 h later, cells were detached with Accumax™
739 (Sigma-Aldrich, A7089) and washed twice with cold PBS on ice. Cells were stained with
740 Annexin V and propidium iodide (PI) according to manufacturer's instruction (BD,
741 556547). Samples were analyzed using an LSRFortessa (BD) flow cytometer, and the
742 fractions of stained cells were quantified using FloJo 10.6, with Staurosporine (4 h, 5 μM)
743 (Tocris, 1285) used as a positive control for cell death and to help establish gating of the
744 sorted cells.

745 **Cystine uptake**

746 Wild-type MEFs were cultured in 6-well plates and serum starved for 23.5 h before
747 rapamycin treatment (20 nM, 30 min) prior to insulin stimulation (500 nM, 24 h). *Tsc2*$^{-/-}$
748 MEFs were cultured in 6-well plates and serum-starved for 16 h in the presence of 20 nM
749 rapamycin or 10 μM erastin (Selleckchem, S7242). Cells were then incubated in the same
750 medium containing 0.1 μCi L-[1, 2, 1', 2'-^{14}C]-Cystine (PerkinElmer, NEC854010UC) for 10
751 min. Cells were washed three times in ice-cold PBS containing cold cystine (1 mM), lysed
752 in Triton lysis buffer, and quantified for radiolabel incorporation with a Beckman LS6500
753 scintillation counter. Cells from identically treated parallel plates were counted using a
754 Beckman Z1-Coulter Counter to normalize cystine uptake data to cell number. *Atf4*$^{-/-}$ cells
755 were serum-starved in the presence of doxycycline (1 μg/mL), 1X MEM NEAA mixture, 1
756 mM cysteine (Sigma, C7477) and either vehicle or rapamycin (20 nM) prior to assaying
757 cystine uptake as above, which was measured for 10 min in DMEM without MEM NEAA
758 and cysteine supplementation.

759 **Measurements of cellular glutathione**

760 Cells were plated in 96-well plates at 5000 cells/well. Total glutathione, GSH, and GSSG
761 levels were measured using the GSH/GSSG-Glo Assay (Promega, V6611) according to
762 the manufacturer's protocol. Total glutathione levels were normalized to cell number
763 determined from parallel plates.

764 For measurements via LC-MS/MS, metabolites were extracted from cells on dry ice using
765 80% methanol, and extracts were dried under nitrogen gas for metabolite profiling via

766 selected reaction monitoring (SRM) with polarity switching using a 5500 QTRAP mass
767 spectrometer. Data were analyzed using MultiQuant 2.1.1 software (AB/SCIEX) to
768 calculate the Q3 peak area. Normalized peak area of glutathione from human *TSC2*$^{-/-}$
769 angiomyolipoma (621-101) cells was determined from data published in (Tang et al.,
770 2019). For *TSC2*$^{-/-}$ ELT3 xenograft studies, experimental details are provided in (Valvezan
771 et al., 2017). Briefly, mice bearing *TSC2*$^{-/-}$ ELT3 xenograft tumors were treated for 5 days
772 with vehicle or rapamycin (1 mg/kg day 1, 3, 5) and tumors were harvested for metabolite
773 extraction, as above, 3 h after the final treatment.

774 **Statistics**

775 For RNA-sequencing analysis, Benjamini-Hochberg FDR-adjusted p values were
776 determined from empirical Bayes moderated t-statistics using the voom and eBayes
777 functions from the limma package. Comparisons with FDR-adjusted $p < 0.05$ were
778 considered significant for the gene groups denoted compared to vehicle-treated controls.
779 For KEGG enrichment and GSEA plots, *P* values were false discovery rate corrected.
780 Unpaired two-tailed t-tests were used for Nanostring analyses to calculate *P* values for
781 rank ordering. All remaining statistical analysis was performed with Prism 8 software
782 (GraphPad Software, La Jolla, California). Statistical analyses for qPCR data with two
783 treatment groups were determined by unpaired two-tailed t-test, while those with greater
784 than two treatment groups, were determined by one-way ANOVA with Holm-Sidak
785 method for multiple comparisons. Statistical analyses for protein synthesis assays were
786 determined by one-way ANOVA with Holm-Sidak method for multiple comparisons from
787 values quantified with ImageJ software (US National Institutes of Health, Bethesda,
788 Maryland). For proliferation assays, unpaired two tailed t-test were used for comparisons
789 to GFP-expressing cells. For cell death analysis, one-way ANOVA with Holm-Sidak
790 method for multiple comparisons, summing the AnnexinV+/PI -, AnnexinV-/PI+, and
791 AnnexinV+/PI+ populations for each conditions. For glutathione quantification from
792 xenograft tumors or Tsc2$^{-/-}$ MEFs with addback of EV or TSC2, an unpaired two tailed t-
793 test was performed. For remaining glutathione assays and all cystine uptake experiments,
794 one-way ANOVA with Holm-Sidak method for multiple comparisons was used.

795 **Source Data**

796 Source data file 1 provides the list of genes depicted in the Venn diagram in Figure 1C.
797 Source data file 2 provides the values depicted in the heatmap shown in Figures 2A, F.
798 The source data for the RNA-sequencing experiment can be found at GEO under the
799 accession number GSE158605.

800 **Acknowledgements**

801 We thank David J. Kwiatkowski, Elizabeth P. Henske, Randal J. Kaufman, and Alex Toker
802 for cell lines and materials and Min Yuan, Gerta Hoxhaj, and Issam Ben-Sahra for
803 technical assistance and critical discussions. This research was supported by grants from
804 the NIH: T32-ES016645 (M.E.T.), F31-CA228332 (M.E.T.), R35-CA197459 (B.D.M.) and
805 P01-CA120964 (B.D.M and J.A.); the Department of Defense's Congressionally Directed
806 Medical Research Program on Tuberous Sclerosis Complex, award no. W81XWH-18-1-
807 0659 (B.D.M.); and a research grant from Zafgen (B.D.M. and J.R.M.).

808 B.D.M. is a shareholder and scientific advisory board member of LAM Therapeutics and
809 Navitor Pharmaceuticals. All other authors declare no competing financial interests.

810 **References**

811 Adams, C. M. (2007). Role of the Transcription Factor ATF4 in the Anabolic Actions of
812 Insulin and the Anti-anabolic Actions of Glucocorticoids. *J Biol Chem, 282*(23),
813 16744-16753. doi:10.1074/jbc.M610510200

814 Arsham, A. M., Plas, D. R., Thompson, C. B., & Simon, M. C. (2002).
815 Phosphatidylinositol 3-kinase/Akt signaling is neither required for hypoxic stabilization
816 of HIF-1 alpha nor sufficient for HIF-1-dependent target gene transcription. *J Biol*
817 *Chem, 277*(17), 15162-15170. doi:10.1074/jbc.M111162200

818 Arts, G.-J., Kuersten, S., Romby, P., Ehresmann, B., & Mattaj, I. W. (1998). The role of
819 exportin-t in selective nuclear export of mature tRNAs. *EMBO J, 17*(24), 7430-7441.
820 doi:10.1093/emboj/17.24.7430

821 Bannai, S., & Kitamura, E. (1980). Transport interaction of L-cystine and L-glutamate in
822 human diploid fibroblasts in culture. *J Biol Chem, 255*(6), 2372-2376.
823 doi:10.1016/0026-0495(87)90207-1
824 Ben-Sahra, I., Hoxhaj, G., Ricoult, S. J. H., Asara, J. M., & Manning, B. D. (2016).
825 mTORC1 induces purine synthesis through control of the mitochondrial
826 tetrahydrofolate cycle. *Science, 351*(6274), 728-733. doi:10.1126/science.aad0489
827 Brugarolas, J. B., Vazquez, F., Reddy, A., Sellers, W. R., & Kaelin Jr, W. G. (2003).
828 TSC2 regulates VEGF through mTOR-dependent and -independent pathways.
829 *Cancer Cell, 4*(2), 147-158. doi:10.1016/S1535-6108(03)00187-9
830 Clemens, M. J. (1996). Protein kinases that phosphorylate eIF2 and eIF2B, and their
831 role in eukaryotic cell translational control. *Translational Control, 30*, 139-172.
832 Cohen, D. M., Won, K.-J., Nguyen, N., Lazar, M. A., Chen, C. S., & Steger, D. J. (2015).
833 ATF4 licenses C/EBPβ activity in human mesenchymal stem cells primed for
834 adipogenesis. *eLife, 4*, e06821. doi:10.7554/eLife.06821
835 Csibi, A., Lee, G., Yoon, S.-O., Tong, H., Ilter, D., Elia, I., Fendt, S.-M., Roberts,
836 Thomas M., & Blenis, J. (2014). The mTORC1/S6K1 Pathway Regulates Glutamine
837 Metabolism through the eIF4B-Dependent Control of c-Myc Translation. *Curr Biol,*
838 *24*(19), 2274-2280. doi:10.1016/j.cub.2014.08.007
839 Dehairs, J., Talebi, A., Cherifi, Y., & Swinnen, J. V. (2016). CRISP-ID: decoding
840 CRISPR mediated indels by Sanger sequencing. *Sci Rep, 6*(1), 28973.
841 doi:10.1038/srep28973
842 Duvel, K., Yecies, J. L., Menon, S., Raman, P., Lipovsky, A. I., Souza, A. L.,
843 Triantafellow, E., Ma, Q., Gorski, R., Cleaver, S., Vander Heiden, M. G., MacKeigan,
844 J. P., Finan, P. M., Clish, C. B., Murphy, L. O., & Manning, B. D. (2010). Activation of
845 a metabolic gene regulatory network downstream of mTOR complex 1. *Mol Cell, 39*.
846 doi:10.1016/j.molcel.2010.06.022
847 Ebert, S. M., Bullard, S. A., Basisty, N., Marcotte, G. R., Skopec, Z. P., Dierdorff, J. M.,
848 Al-Zougbi, A., Tomcheck, K. C., DeLau, A. D., Rathmacher, J. A., Bodine, S. C.,
849 Schilling, B., & Adams, C. M. (2020). Activating transcription factor 4 (ATF4)
850 promotes skeletal muscle atrophy by forming a heterodimer with the transcriptional
851 regulator C/EBPβ. *J Biol Chem, 295*(9), 2787-2803. doi:10.1074/jbc.RA119.012095

852 Gachon, F., Gaudray, G., Thébault, S., Basbous, J., Koffi, J. A., Devaux, C., & Mesnard,
853 J. (2001). The cAMP response element binding protein-2 (CREB-2) can interact with
854 the C/EBP-homologous protein (CHOP). *FEBS Lett, 502*(1-2), 57-62.
855 doi:10.1016/s0014-5793(01)02646-1
856 Griffith, O. W., & Meister, A. (1979). Potent and specific inhibition of glutathione
857 synthesis by buthionine sulfoximine (S-n-butyl homocysteine sulfoximine). *J Biol*
858 *Chem, 254*(16), 7558-7560.
859 Gu, Y., Albuquerque, C. P., Braas, D., Zhang, W., Villa, G. R., Bi, J., Ikegami, S., Masui,
860 K., Gini, B., Yang, H., Gahman, T. C., Shiau, A. K., Cloughesy, T. F., Christofk, H. R.,
861 Zhou, H., Guan, K. L., & Mischel, P. S. (2017). mTORC2 Regulates Amino Acid
862 Metabolism in Cancer by Phosphorylation of the Cystine-Glutamate Antiporter xCT.
863 *Mol Cell, 67*(1), 128-138.e127. doi:10.1016/j.molcel.2017.05.030
864 Guangchuang Yu, L.-G. W., Yanyan Han, and Qing-Yu He. (2012). clusterProfiler: an R
865 Package for Comparing Biological Themes Among Gene Clusters. *OMICS: A Journal*
866 *of Integrative Biology, 16*(5), 284-287. doi:10.1089/omi.2011.0118
867 Habib, E., Linher-Melville, K., Lin, H. X., & Singh, G. (2015). Expression of xCT and
868 activity of system xc(-) are regulated by NRF2 in human breast cancer cells in
869 response to oxidative stress. *Redox Biol, 5*, 33-42. doi:10.1016/j.redox.2015.03.003
870 Han, J., Back, S. H., Hur, J., Lin, Y.-H., Gildersleeve, R., Shan, J., Yuan, C. L.,
871 Krokowski, D., Wang, S., Hatzoglou, M., Kilberg, M. S., Sartor, M. A., & Kaufman, R.
872 J. (2013). ER-stress-induced transcriptional regulation increases protein synthesis
873 leading to cell death. *Nat Cell Biol, 15*(5), 481-490. doi:10.1038/ncb2738
874 Harding, H. P., Novoa, I., Zhang, Y., Zeng, H., Wek, R., Schapira, M., & Ron, D. (2000).
875 Regulated Translation Initiation Controls Stress-Induced Gene Expression in
876 Mammalian Cells. *Mol Cell, 6*(5), 1099-1108. doi:10.1016/S1097-2765(00)00108-8
877 Harding, H. P., Zhang, Y., Zeng, H., Novoa, I., Lu, P. D., Calfon, M., Sadri, N., Yun, C.,
878 Popko, B., Paules, R., Stojdl, D. F., Bell, J. C., Hettmann, T., Leiden, J. M., & Ron, D.
879 (2003). An integrated stress response regulates amino acid metabolism and
880 resistance to oxidative stress. *Mol Cell, 11*(3), 619-633. doi:10.1016/S1097-
881 2765(03)00105-9

He, C. H., Gong, P., Hu, B., Stewart, D., Choi, M. E., Choi, A. M., & Alam, J. (2001). Identification of activating transcription factor 4 (ATF4) as an Nrf2-interacting protein. Implication for heme oxygenase-1 gene regulation. *J Biol Chem, 276*(24), 20858-20865. doi:10.1074/jbc.M101198200

Heigwer, F., Kerr, G., & Boutros, M. (2014). E-CRISP: fast CRISPR target site identification. *Nat Methods, 11*(2), 122-123. doi:10.1038/nmeth.2812

Hodges, L. C., Houston, K. D., Hunter, D. S., Fuchs-Young, R., Zhang, Z., Wineker, R. C., & Walker, C. L. (2002). Transdominant suppression of estrogen receptor signaling by progesterone receptor ligands in uterine leiomyoma cells. *Mol Cell Endocrinol, 196*(1-2), 11-20. doi:10.1016/s0303-7207(02)00230-7

Holz, M. K., Ballif, B. A., Gygi, S. P., & Blenis, J. (2005). mTOR and S6K1 Mediate Assembly of the Translation Preinitiation Complex through Dynamic Protein Interchange and Ordered Phosphorylation Events. *Cell, 123*(4), 569-580. doi:10.1016/j.cell.2005.10.024

Horton, J. D., Goldstein, J. L., & Brown, M. S. (2002). SREBPs: activators of the complete program of cholesterol and fatty acid synthesis in the liver. *J Clin Invest, 109*(9), 1125-1131. doi:10.1172/JCI15593

Hudson, C. C., Liu, M., Chiang, G. G., Otterness, D. M., Loomis, D. C., Kaper, F., Giaccia, A. J., & Abraham, R. T. (2002). Regulation of hypoxia-inducible factor 1α expression and function by the mammalian target of rapamycin. *Mol Cell Biol, 22*(20), 7004-7014. doi:10.1128/mcb.22.20.7004-7014.2002

Jefferies, H. B., Reinhard, C., Kozma, S. C., & Thomas, G. (1994). Rapamycin selectively represses translation of the "polypyrimidine tract" mRNA family. *PNAS, 91*(10), 4441-4445. doi:10.1073/pnas.91.10.4441

Kong, H., & Chandel, N. S. (2018). Regulation of redox balance in cancer and T cells. *J Biol Chem, 293*(20), 7499-7507. doi:10.1074/jbc.TM117.000257

Kutay, U., Lipowsky, G., Izaurralde, E., Bischoff, F. R., Schwarzmaier, P., Hartmann, E., & Görlich, D. (1998). Identification of a tRNA-Specific Nuclear Export Receptor. *Mol Cell, 1*(3), 359-369. doi:10.1016/S1097-2765(00)80036-2

Lam, H. C., Baglini, C. V., Lope, A. L., Parkhitko, A. A., Liu, H.-J., Alesi, N., Malinowska, I. A., Ebrahimi-Fakhari, D., Saffari, A., Yu, J. J., Pereira, A., Khabibullin, D., Ogorek,

913 B., Nijmeh, J., Kavanagh, T., Handen, A., Chan, S. Y., Asara, J. M., Oldham, W. M.,
914 Diaz-Meco, M. T., Moscat, J., Sahin, M., Priolo, C., & Henske, E. P. (2017).
915 p62/SQSTM1 Cooperates with Hyperactive mTORC1 to Regulate Glutathione
916 Production, Maintain Mitochondrial Integrity, and Promote Tumorigenesis. *Cancer*
917 *Res, 77*(12), 3255. doi:10.1158/0008-5472.CAN-16-2458
918 Lange, P. S., Chavez, J. C., Pinto, J. T., Coppola, G., Sun, C.-W., Townes, T. M.,
919 Geschwind, D. H., & Ratan, R. R. (2008). ATF4 is an oxidative stress-inducible,
920 prodeath transcription factor in neurons in vitro and in vivo. *J Exp Med, 205*(5), 1227-
921 1242. doi:10.1084/jem.20071460
922 Laughner, E., Taghavi, P., Chiles, K., Mahon, P. C., & Semenza, G. L. (2001). HER2
923 (neu) signaling increases the rate of hypoxia-inducible factor 1α (HIF-1α) synthesis:
924 novel mechanism for HIF-1-mediated vascular endothelial growth factor expression.
925 *Mol Cell Biol, 21*(12), 3995-4004. doi:10.1128/mcb.21.12.3995-4004.2001
926 Li, C., Chen, H., Lan, Z., He, S., Chen, R., Wang, F., Liu, Z., Li, K., Cheng, L., Liu, Y.,
927 Sun, K., Wan, X., Chen, X., Peng, H., Li, L., Zhang, Y., Jing, Y., Huang, M., Wang,
928 Y., Wang, Y., Jiang, J., Zha, X., Chen, L., & Zhang, H. (2019). mTOR-dependent
929 upregulation of xCT blocks melanin synthesis and promotes tumorigenesis. *Cell*
930 *Death & Diff, 26*(10), 2015-2028. doi:10.1038/s41418-019-0274-0
931 Liao, Y., Smyth, G. K., & Shi, W. (2019). The R package Rsubread is easier, faster,
932 cheaper and better for alignment and quantification of RNA sequencing reads.
933 *Nucleic Acids Res, 47*(8), e47. doi:10.1093/nar/gkz114
934 Lien, E. C., Ghisolfi, L., Geck, R. C., Asara, J. M., & Toker, A. (2017). Oncogenic PI3K
935 promotes methionine dependency in breast cancer cells through the cystine-
936 glutamate antiporter xCT. *Sci Sig, 10*(510), eaao6604. doi:10.1126/scisignal.aao6604
937 Ma, X. M., & Blenis, J. (2009). Molecular mechanisms of mTOR-mediated translational
938 control. *Nat Rev Mol Cell Biol, 10*(5), 307-318. doi:10.1038/nrm2672
939 Meister, A. (1983). Selective Modification of Glutathione Metabolism. *Science,*
940 *220*(4596), 472-477. doi:10.1126/science.6836290
941 Nakazawa, M. S., Keith, B., & Simon, M. C. (2016). Oxygen availability and metabolic
942 adaptations. *Nat Rev Cancer, 16*(10), 663-673. doi:10.1038/nrc.2016.84

943 Newman, J. R. S., & Keating, A. E. (2003). Comprehensive Identification of Human
944 bZIP Interactions with Coiled-Coil Arrays. *Science, 300*(5628), 2097.
945 doi:10.1126/science.1084648
946 Owen, J. L., Zhang, Y., Bae, S.-H., Farooqi, M. S., Liang, G., Hammer, R. E., Goldstein,
947 J. L., & Brown, M. S. (2012). Insulin stimulation of SREBP-1c processing in
948 transgenic rat hepatocytes requires p70 S6-kinase. *PNAS, 109*(40), 16184.
949 doi:10.1073/pnas.1213343109
950 Ozcan, U., Ozcan, L., Yilmaz, E., Düvel, K., Sahin, M., Manning, B. D., & Hotamisligil,
951 G. S. (2008). Loss of the Tuberous Sclerosis Complex Tumor Suppressors Triggers
952 the Unfolded Protein Response to Regulate Insulin Signaling and Apoptosis. *Mol*
953 *Cell, 29*(5), 541-551. doi:10.1016/j.molcel.2007.12.023
954 Park, Y., Reyna-Neyra, A., Philippe, L., & Thoreen, C. C. (2017). mTORC1 Balances
955 Cellular Amino Acid Supply with Demand for Protein Synthesis through Post-
956 transcriptional Control of ATF4. *Cell Rep, 19*(6), 1083-1090.
957 doi:10.1016/j.celrep.2017.04.042
958 Peterson, Timothy R., Sengupta, Shomit S., Harris, Thurl E., Carmack, Anne E., Kang,
959 Seong A., Balderas, E., Guertin, David A., Madden, Katherine L., Carpenter, Anne E.,
960 Finck, Brian N., & Sabatini, David M. (2011). mTOR Complex 1 Regulates Lipin 1
961 Localization to Control the SREBP Pathway. *Cell, 146*(3), 408-420.
962 doi:10.1016/j.cell.2011.06.034
963 Porstmann, T., Santos, C. R., Griffiths, B., Cully, M., Wu, M., Leevers, S., Griffiths, J. R.,
964 Chung, Y.-L., & Schulze, A. (2008). SREBP activity is regulated by mTORC1 and
965 contributes to Akt-dependent cell growth. *Cell Metab, 8*(3), 224-236.
966 doi:10.1016/j.cmet.2008.07.007
967 Ran, F. A., Hsu, P. D., Wright, J., Agarwala, V., Scott, D. A., & Zhang, F. (2013).
968 Genome engineering using the CRISPR-Cas9 system. *Nat Protoc, 8*(11), 2281-2308.
969 doi:10.1038/nprot.2013.143
970 Raught, B., Peiretti, F., Gingras, A. C., Livingstone, M., Shahbazian, D., Mayeur, G. L.,
971 Polakiewicz, R. D., Sonenberg, N., & Hershey, J. W. (2004). Phosphorylation of
972 eucaryotic translation initiation factor 4B Ser422 is modulated by S6 kinases. *EMBO*
973 *J, 23*(8), 1761-1769. doi:10.1038/sj.emboj.7600193

974 Ritchie, M. E., Phipson, B., Wu, D., Hu, Y., Law, C. W., Shi, W., & Smyth, G. K. (2015).
975 limma powers differential expression analyses for RNA-sequencing and microarray
976 studies. *Nucleic Acids Res, 43*(7), e47. doi:10.1093/nar/gkv007
977 Robinson, M. D., McCarthy, D. J., & Smyth, G. K. (2009). edgeR: a Bioconductor
978 package for differential expression analysis of digital gene expression data.
979 *Bioinformatics, 26*(1), 139-140. doi:10.1093/bioinformatics/btp616
980 Sabò, A., Kress, T. R., Pelizzola, M., de Pretis, S., Gorski, M. M., Tesi, A., Morelli, M. J.,
981 Bora, P., Doni, M., Verrecchia, A., Tonelli, C., Fagà, G., Bianchi, V., Ronchi, A., Low,
982 D., Müller, H., Guccione, E., Campaner, S., & Amati, B. (2014). Selective
983 transcriptional regulation by Myc in cellular growth control and lymphomagenesis.
984 *Nature, 511*(7510), 488-492. doi:10.1038/nature13537
985 Sasaki, H., Sato, H., Kuriyama-Matsumura, K., Sato, K., Maebara, K., Wang, H.,
986 Tamba, M., Itoh, K., Yamamoto, M., & Bannai, S. (2002). Electrophile Response
987 Element-mediated Induction of the Cystine/Glutamate Exchange Transporter Gene
988 Expression. *J Biol Chem, 277*(47), 44765-44771. doi:10.1074/jbc.M208704200
989 Scheuner, D., Song, B., McEwen, E., Liu, C., Laybutt, R., Gillespie, P., Saunders, T.,
990 Bonner-Weir, S., & Kaufman, R. J. (2001). Translational control is required for the
991 unfolded protein response and in vivo glucose homeostasis. *Mol Cell, 7*(6), 1165-
992 1176. doi:10.1016/S1097-2765(01)00265-9
993 Schuhmacher, M., & Eick, D. (2013). Dose-dependent regulation of target gene
994 expression and cell proliferation by c-Myc levels. *Transcription, 4*(4), 192-197.
995 doi:10.4161/trns.25907
996 Subramanian, A., Tamayo, P., Mootha, V. K., Mukherjee, S., Ebert, B. L., Gillette, M. A.,
997 Paulovich, A., Pomeroy, S. L., Golub, T. R., Lander, E. S., & Mesirov, J. P. (2005).
998 Gene set enrichment analysis: A knowledge-based approach for interpreting
999 genome-wide expression profiles. *PNAS, 102*(43), 15545.
1000 doi:10.1073/pnas.0506580102
1001 Tang, Y., El-Chemaly, S., Taveira-Dasilva, A., Goldberg, H. J., Bagwe, S., Rosas, I. O.,
1002 Moss, J., Priolo, C., & Henske, E. P. (2019). Alterations in Polyamine Metabolism in
1003 Patients With Lymphangioleiomyomatosis and Tuberous Sclerosis Complex 2-
1004 Deficient Cells. *Chest, 156*(6), 1137-1148. doi:10.1016/j.chest.2019.05.038

1005 Thomas, G. V., Tran, C., Mellinghoff, I. K., Welsbie, D. S., Chan, E., Fueger, B.,
1006 Czernin, J., & Sawyers, C. L. (2006). Hypoxia-inducible factor determines sensitivity
1007 to inhibitors of mTOR in kidney cancer. *Nat Med, 12*(1), 122-127.
1008 doi:10.1038/nm1337
1009 Thoreen, C. C., Chantranupong, L., Keys, H. R., Wang, T., Gray, N. S., & Sabatini, D.
1010 M. (2012). A unifying model for mTORC1-mediated regulation of mRNA translation.
1011 *Nature, 485*(7396), 109-113. doi:10.1038/nature11083
1012 Torrence, M. E., & Manning, B. D. (2018). Nutrient Sensing in Cancer. *Ann Rev of*
1013 *Cancer Biol, 2*(1), 251-269. doi:10.1146/annurev-cancerbio-030617-050329
1014 Vallejo, M., Ron, D., Miller, C. P., & Habener, J. F. (1993). C/ATF, a member of the
1015 activating transcription factor family of DNA-binding proteins, dimerizes with
1016 CAAT/enhancer-binding proteins and directs their binding to cAMP response
1017 elements. *PNAS, 90*(10), 4679. doi:10.1073/pnas.90.10.4679
1018 Valvezan, A. J., & Manning, B. D. (2019). Molecular logic of mTORC1 signalling as a
1019 metabolic rheostat. *Nat Metab, 1*(3), 321-333. doi:10.1038/s42255-019-0038-7
1020 Valvezan, A. J., Turner, M., Belaid, A., Lam, H. C., Miller, S. K., McNamara, M. C.,
1021 Baglini, C., Housden, B. E., Perrimon, N., Kwiatkowski, D. J., Asara, J. M., Henske,
1022 E. P., & Manning, B. D. (2017). mTORC1 Couples Nucleotide Synthesis to
1023 Nucleotide Demand Resulting in a Targetable Metabolic Vulnerability. *Cancer Cell,*
1024 *32*(5), 624-638.e625. doi:10.1016/j.ccell.2017.09.013
1025 Vattem, K. M., & Wek, R. C. (2004). Reinitiation involving upstream ORFs regulates
1026 ATF4 mRNA translation in mammalian cells. *PNAS, 101*(31), 11269-11274.
1027 doi:10.1073/pnas.0400541101
1028 Wall, M., Poortinga, G., Hannan, K. M., Pearson, R. B., Hannan, R. D., & McArthur, G.
1029 A. (2008). Translational control of c-MYC by rapamycin promotes terminal myeloid
1030 differentiation. *Blood, 112*(6), 2305-2317. doi:10.1182/blood-2007-09-111856
1031 Walter, P., & Ron, D. (2011). The Unfolded Protein Response: From Stress Pathway to
1032 Homeostatic Regulation. *Science, 334*(6059), 1081. doi:10.1126/science.1209038
1033 Walz, S., Lorenzin, F., Morton, J., Wiese, K. E., von Eyss, B., Herold, S., Rycak, L.,
1034 Dumay-Odelot, H., Karim, S., Bartkuhn, M., Roels, F., Wüstefeld, T., Fischer, M.,
1035 Teichmann, M., Zender, L., Wei, C.-L., Sansom, O., Wolf, E., & Eilers, M. (2014).

1036 Activation and repression by oncogenic MYC shape tumour-specific gene expression
1037 profiles. *Nature, 511*(7510), 483-487. doi:10.1038/nature13473
1038 Yang, W. S., & Stockwell, B. R. (2008). Synthetic Lethal Screening Identifies
1039 Compounds Activating Iron-Dependent, Nonapoptotic Cell Death in Oncogenic-RAS-
1040 Harboring Cancer Cells. *Chem Biol, 15*(3), 234-245.
1041 doi:10.1016/j.chembiol.2008.02.010
1042 Ye, P., Mimura, J., Okada, T., Sato, H., Liu, T., Maruyama, A., Ohyama, C., & Itoh, K.
1043 (2014). Nrf2- and ATF4-Dependent Upregulation of xCT Modulates the Sensitivity of
1044 T24 Bladder Carcinoma Cells to Proteasome Inhibition. *Mol Cell Biol, 34*(18), 3421.
1045 doi:10.1128/MCB.00221-14
1046 Zarei, M., Du, H., Nassar, A. H., Yan, R. E., Giannikou, K., Johnson, S. H., Lam, H. C.,
1047 Henske, E. P., Wang, Y., Zhang, T., Asara, J., & Kwiatkowski, D. J. (2019). Tumors
1048 with TSC mutations are sensitive to CDK7 inhibition through NRF2 and glutathione
1049 depletion. *J Exp Med, 216*(11), 2635-2652. doi:10.1084/jem.20190251
1050 Zhang, Y., Nicholatos, J., Dreier, J. R., Ricoult, S. J. H., Widenmaier, S. B., Hotamisligil,
1051 G. S., Kwiatkowski, D. J., & Manning, B. D. (2014). Coordinated regulation of protein
1052 synthesis and degradation by mTORC1. *Nature, 513*(7518), 440-443.
1053 doi:10.1038/nature13492
1054 Zhong, H., Chiles, K., Feldser, D., Laughner, E., Hanrahan, C., Georgescu, M. M.,
1055 Simons, J. W., & Semenza, G. L. (2000). Modulation of hypoxia-inducible factor
1056 1alpha expression by the epidermal growth factor/phosphatidylinositol 3-
1057 kinase/PTEN/AKT/FRAP pathway in human prostate cancer cells: implications for
1058 tumor angiogenesis and therapeutics. *Cancer Res, 60*(6), 1541-1545.
1059 Zirin, J., Ni, X., Sack, L. M., Yang-Zhou, D., Hu, Y., Brathwaite, R., Bulyk, M. L.,
1060 Elledge, S. J., & Perrimon, N. (2019). Interspecies analysis of MYC targets identifies
1061 tRNA synthetases as mediators of growth and survival in MYC-overexpressing cells.
1062 *PNAS, 116*(29), 14614. doi:10.1073/pnas.1821863116

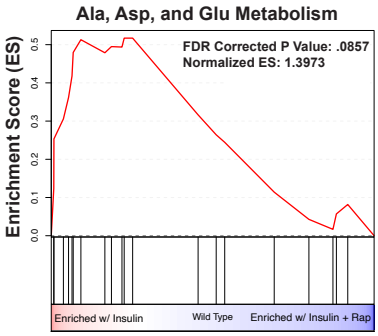

Supplemental Figure 1. mTORC1 signaling activates a subset of ATF4-dependent genes also activated by the integrated stress response, related to Figure 1. GSEA plot of alanine, aspartate, and glutamate metabolism genes. *P* values were FDR corrected and enrichment scores (ES) were normalized to total read count.

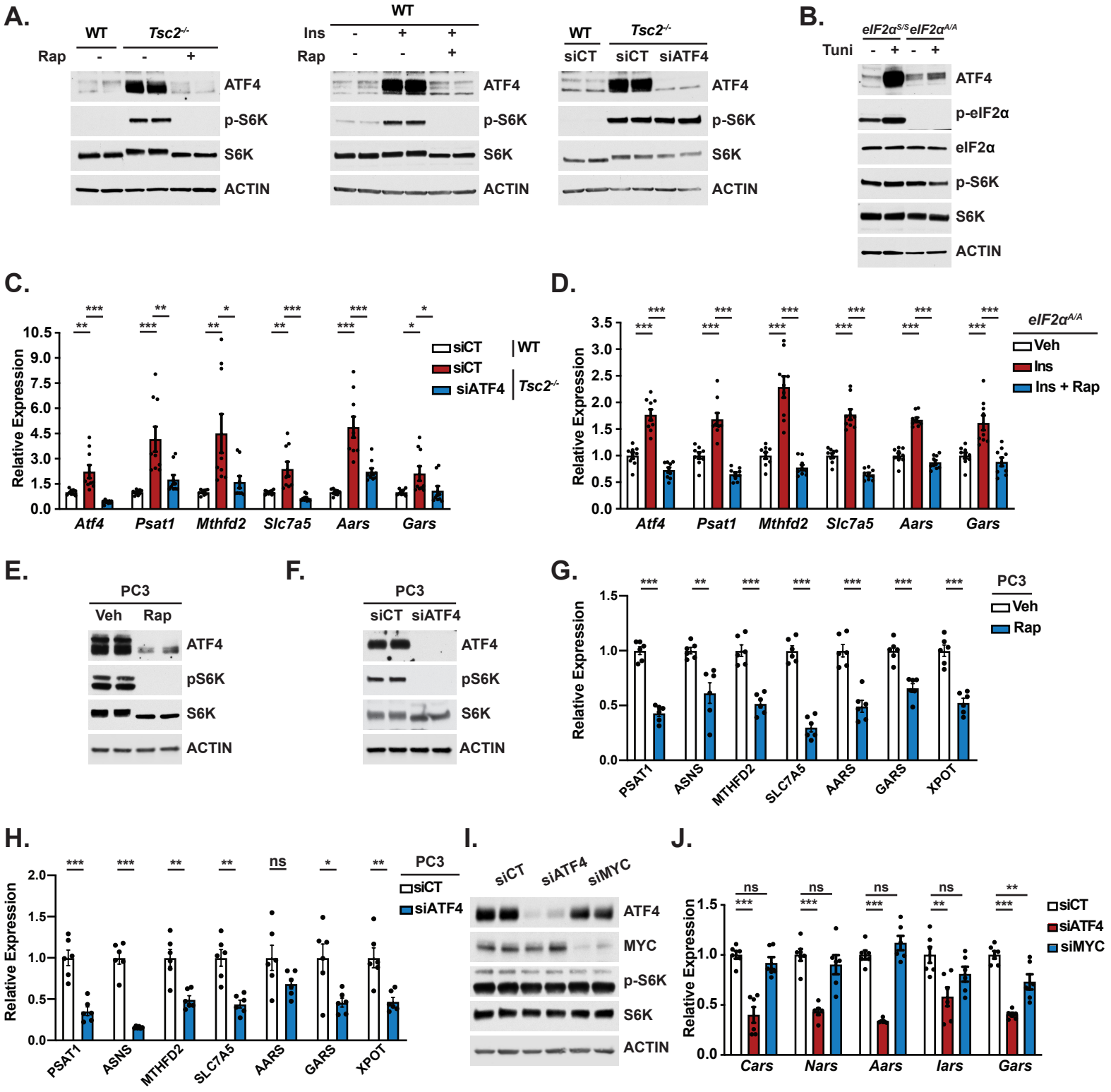
A.
WT
Tsc2-/-
Rap
ATF4
p-S6K
S6K
ACTIN
WT
Ins
Rap
WT
Tsc2-/-
siCT
siCT
siATF4
B.
eIF2αS/S
eIF2αA/A
Tuni
ATF4
p-eIF2α
eIF2α
p-S6K
S6K
ACTIN
C.
Relative Expression
siCT
siCT
siATF4
WT
Tsc2-/-
Atf4
Psat1
Mthfd2
Slc7a5
Aars
Gars
D.
Relative Expression
eIF2αA/A
Veh
Ins
Ins + Rap
Atf4
Psat1
Mthfd2
Slc7a5
Aars
Gars
E.
PC3
Veh
Rap
ATF4
pS6K
S6K
ACTIN
F.
PC3
siCT
siATF4
ATF4
pS6K
S6K
ACTIN
G.
Relative Expression
PC3
Veh
Rap
PSAT1
ASNS
MTHFD2
SLC7A5
AARS
GARS
XPOT
H.
Relative Expression
PC3
siCT
siATF4
PSAT1
ASNS
MTHFD2
SLC7A5
AARS
GARS
XPOT
I.
siCT
siATF4
siMYC
ATF4
MYC
p-S6K
S6K
ACTIN
J.
Relative Expression
siCT
siATF4
siMYC
Cars
Nars
Aars
Iars
Gars

1067 **Supplemental Figure 2. mTORC1 and ATF4 regulate genes involved in amino acid**
1068 **synthesis, transport, and charging, related to Figure 2**.
1069 (A) Representative immunoblots corresponding to Nanostring heatmaps depicted in
1070 Figure 2A with biological duplicates shown.
1071 (B) Representative immunoblot of *eIF2*$\alpha^{A/A}$ MEFs treated with vehicle or tunicamycin (2
1072 µg/mL, 4 h).
1073 (C,D) qPCR analysis of the indicated transcripts in *Tsc2*$^{+/+}$ (WT) and *Tsc2*$^{-/-}$ MEFs treated
1074 as described in Figure 2A (C) or in eIF2$\alpha^{A/A}$ MEFs treated as described in Figure 2F (D).
1075 Expression relative to non-targeting control transfected (C) or vehicle-treated,
1076 unstimulated WT cells (D) is graphed as mean ± SEM from three independent
1077 experiments, each with 3 biological replicates (n=9).
1078 (E,F) Representative immunoblots of serum-deprived PC3 cells treated with vehicle or
1079 rapamycin (20 nM, 16 h) (E) or transfected with *Atf4* siRNAs or non-targeting controls
1080 (siCT) prior to serum-deprivation (16h) (F) and biological duplicates for each condition
1081 are shown.
1082 (G,H) qPCR analysis of the indicated transcripts treated as in Supplemental figure 2 E, F.
1083 Expression relative to vehicle-treated, unstimulated cells or non-targeting control
1084 transfected cells is graphed as mean ± SEM from three independent experiments, each
1085 with 3 biological replicates (n=9).
1086 (I) Representative immunoblot of *Tsc2*$^{-/-}$ MEFs transfected with *Atf4, Myc*, or non-targeting
1087 controls prior to 16 h of serum-starvation.
1088 (J) qPCR analysis of the indicated transcripts in cells transfected as described in (I).
1089 Expression relative to non-targeting control transfected cells is graphed as mean ± SEM
1090 from two independent experiments, each with 3 biological replicates (n=6).
1091 (A,B,E,F,I) are representative of at least two independent experiments. *$p < .05$, **$p <$
1092 $.01$, ***$p < .001$, ns = not significant, calculated in (C,D,J) via one-way ANOVA with Holm-
1093 Sidak method for multiple comparisons and (G,H) via unpaired two tailed t-test.

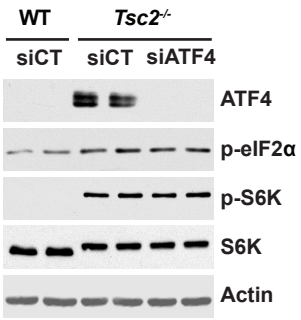

1094 **Supplemental Figure 3. Phosphorylation of eIF2α does not change with siRNA-**
1095 **mediated knockdown of *Atf4* in *Tsc2*$^{-/-}$ MEFs, related to Figure 4.**
1096 Representative immunoblot of *Tsc2*$^{-/-}$ MEFs transfected with *Atf4, Rheb*, or non-targeting
1097 control siRNAs prior to serum starvation for 16h. Data is representative of at least three
1098 independent experiments.

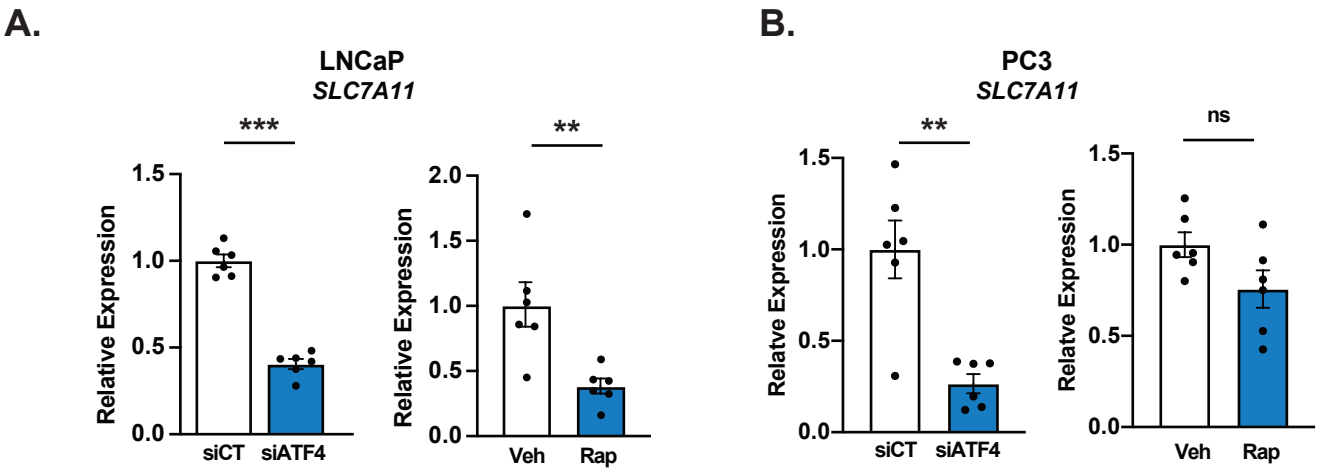

Supplemental Figure 4. mTORC1 regulates cystine uptake necessary for proliferation of *Tsc2*$^{-/-}$ *Atf4*$^{-/-}$ MEFs, related to Figure 5.

(A,B) qPCR analysis of *SLC7A11* in LNCaP or PC3 cells transfected with siRNAs targeting *ATF4* or non-targeting controls (siCT) prior to serum-deprivation in the presence of rapamycin (20 nM, 16 h). Expression relative to non-targeting control transfected cells is graphed as mean ± SEM from two independent experiments, each with 3 biological replicates (n=6).

*p < .05, **p < .01, ***p < .001, ns = not significant, calculated for (A,B) via unpaired two tailed t-test.

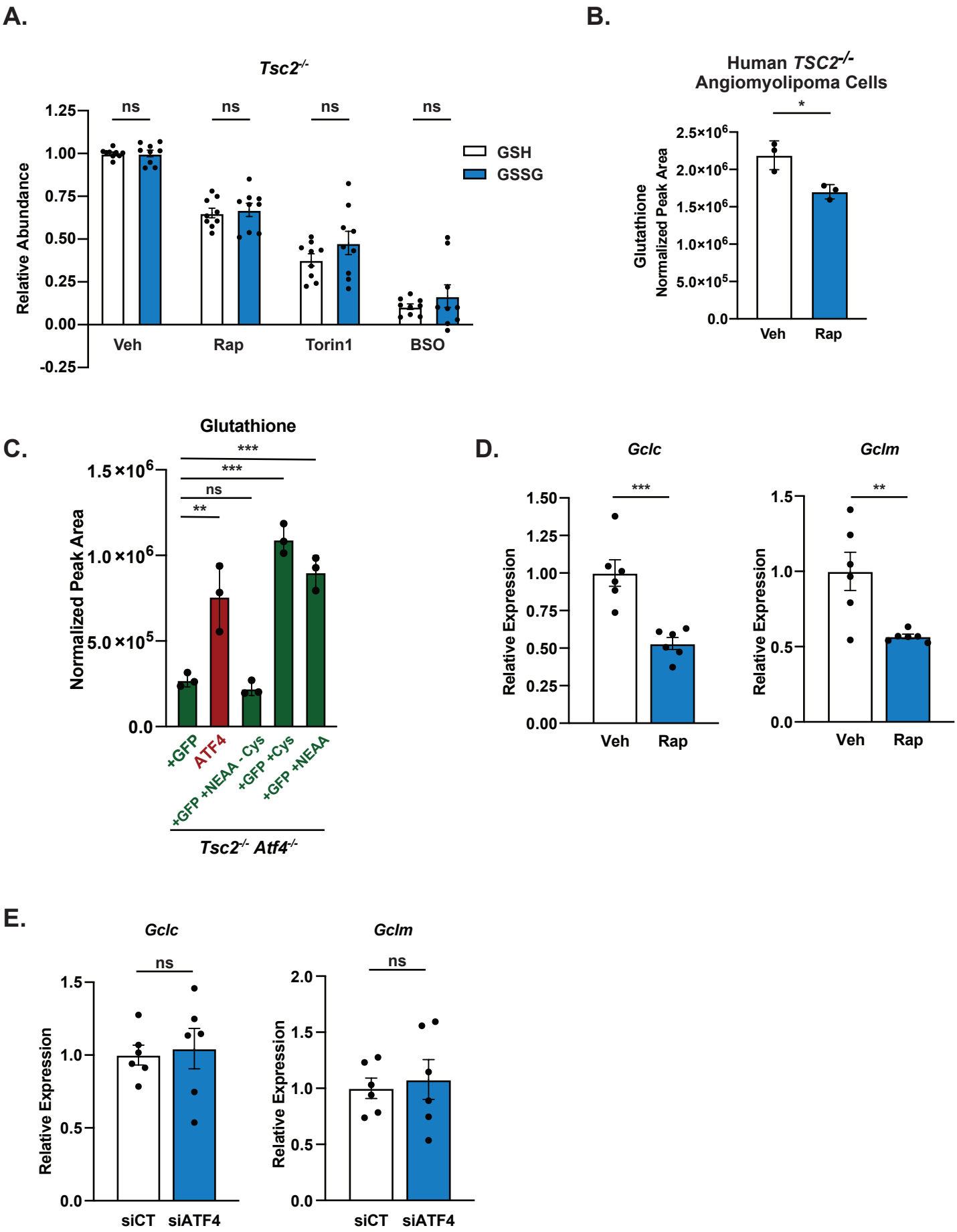
A.
Tsc2-/-
Relative Abundance
1.25
1.00
0.75
0.50
0.25
0.00
-0.25
ns
ns
ns
ns
GSH
GSSG
Veh
Rap
Torin1
BSO
B.
Human TSC2-/-
Angiomyolipoma Cells
Glutathione
Normalized Peak Area
2.5×10^6
2.0×10^6
1.5×10^6
1.0×10^6
5.0×10^5
0.0
*
Veh
Rap
C.
Glutathione
Normalized Peak Area
1.5×10^6
1.0×10^6
5.0×10^5
0.0
***
***
ns
**
+GFP
ATF4
+GFP +NEAA - Cys
+GFP +Cys
+GFP +NEAA
Tsc2-/- Atf4-/-
D.
Gclc
Gclm
Relative Expression
1.50
1.25
1.00
0.75
0.50
0.25
0.00
***
1.5
1.0
0.5
0.0
**
Veh
Rap
E.
Gclc
Gclm
Relative Expression
1.5
1.0
0.5
0.0
ns
2.0
1.5
1.0
0.5
0.0
ns
siCT
siATF4

1108 **Supplemental Figure 5. mTORC1 regulates glutathione levels through ATF4,**
1109 **related to Figure 6.**
1110 (A) Relative GSH and GSSG levels in serum-deprived *Tsc2*$^{-/-}$ MEFs treated with
1111 rapamycin (20 nM,16 h), Torin1 (250 nM, 16 h), or BSO (10 μM, 16 h). GSH and GSSG
1112 levels relative to vehicle-treated cells are graphed as mean ± SEM from three
1113 independent experiments, with 3 biological replicates each (n=9).
1114 (B) Total glutathione levels in human *TSC2*$^{-/-}$ angiomyolipoma cells treated with vehicle
1115 or rapamycin (20 nM, 24 h) measured by LC-MS/MS (mean ± SD, n=3).
1116 (C) Normalized peak area of reduced glutathione from LC-MS/MS analysis of serum-
1117 deprived *Tsc2*$^{-/-}$ *Atf4*$^{-/-}$ MEFs with addback of GFP or ATF4 in the presence of
1118 supplemented cysteine (1 mM), non-essential amino acids without cysteine (100 μM
1119 each), or nonessential amino acids (1 mM cysteine or 100 μM) (mean ± SD, n=3).
1120 (D,E) Transcript abundance of *Gclc* and *Gclm* in *Tsc2*$^{-/-}$ MEFs serum-starved in the
1121 presence of rapamycin (20 nM, 16 h) (D) or transfected with siRNAs targeting *Atf4* or non-
1122 targeting controls prior to serum-deprivation for 16 h (E). Expression relative to vehicle
1123 (D) or non-targeting control transfected cells (E) is graphed as mean ± SEM from two
1124 independent experiments, each with 3 biological replicates (n=6).
1125 (C) is representative of two independent experiments. *p < .05, **p < .01, ***p < .001, ns
1126 = not significant calculated for (A,C) via one-way ANOVA with Holm-Sidak method for
1127 multiple comparisons and unpaired two tailed t-test for (B,D,E).